Received: 9 February 2020 | Revised: 9 September 2020 | Accepted: 12 October 2020

DOI: 10.1002/2050-7038.12688

RESEARCH ARTICLE

WILEY

Model predictive control with technique for order of preference by similarity to ideal solution method for four leg distribution static compensator to improve power quality and reduce switching frequency

Pranay Kumar Alladi | **Siva Kumar Ganjikunta** | **Sreenivasarao Dharmavarapu**

Electrical Engineering Department, National Institute of Technology Warangal, Warangal, India

Correspondence
Siva Kumar Ganjikunta, Electrical Engineering Department, National Institute of Technology Warangal, Warangal, Telangana, India.
Email: gsivakumar@nitw.ac.in

Handling Editor: Rezkallah Miloud

Summary

In this paper, model predictive control (MPC) of four leg distribution static compensator (FL-DSTATCOM) is proposed to compensate the power quality issues and to reduce the higher neutral leg switching frequency of FL-DSTATCOM. Current control using conventional MPC, selects a switching state which will minimize the single constraint cost function, comprising the difference between reference and actual DSTATCOM currents. However, FL-DSTATCOM has a limitation of higher neutral leg switching frequency, and it can be reduced by adding an additional constraint to the cost function using a weighting factor. The reduction in neutral leg switching frequency also reduces the switching frequency of phase leg switches. But, the selection of weighting factor during multiple constraint case is a cumbersome task. Therefore, to simplify the weighting factor selection process, an optimization technique, namely, the technique for order of preference by similarity to ideal solution (TOPSIS) is applied, which further selects the optimal switching state. At the same time, compensation using FL-DSTATCOM mainly depends on reference current extraction and it is a challenging task during unbalance and distortions in supply voltages. To address this problem, an improved conductance factor-based approach is implemented in this paper, which makes reference current extraction simpler, effective and easy to interpret. The efficacy of the proposed method is evaluated using simulation and experimental studies.

List of Abbreviations: MPC, model predictive control; DSTATCOM, distribution static compensator; FL-DSTATCOM, four leg distribution static compensator; TOPSIS, technique for order of preference by similarity to ideal solution; DC, direct current; HB, h bridge; TPSC, three-phase split-capacitor; 3P4W, three-phase four-wire; MCDM, multi-criteria decision making; HF, harmonic free; PFC, power factor correction; PCC, point of common coupling; THD, total harmonic distortion; RMS, root mean square; VIKOR, vlsekriterijumska optimizacija i kompromisno resenje method; LEM, liaisons electroniques et mecaniques.

List of Symbols: vsabc, PCC voltages; ilabc, Load currents; icabc, DSTATCOM currents; Vdc, DC link voltage; vc, Inverter output voltage; C1 and C2, Individual cost functions; λ, Weighting Factor in conventional method; σ1, Weight assigned to cost function 1; σ2, Weight assigned to cost function 2; Q, Closeness Coefficient; Ga, Gb, and Gc, Conductance factors; Ts, Sampling Time; upa, upb, and upc, In-phase unit vectors; Vsm, Amplitude of PCC voltage; vsp(t), In-phase voltage; vsq(t), Quadrature voltage; vsap+, vsbp+, and vscp+, Fundamental positive sequence voltages; Ilpm, Average value of fundamental active component of load current; Ism*, Amplitude of reference source current; Lf, Interfacing inductance; Cdc, DC link capacitance.

KEYWORDS

conductance factor, DSTATCOM, harmonic compensation, model predictive control, weighting factor simplification

1 | INTRODUCTION

Power quality is defined as the competence of a grid or an electric network to supply clean and stable electric power to consumers. Power quality issues are mainly classified as current and voltage related issues.[1] Extensive and continuous research in the area of power electronic devices enables one to use them in commercial, industrial, residential, transportation and utility systems. In the distribution system, power electronic devices present in customer loads are the fundamental reason for non-linear and harmonic currents. The major sources of neutral current are unbalanced loads and triplen harmonic currents generated by computer loads. This neutral current is increasing the burden on the neutral wire and sometimes it leads to breakdown of neutral wire.[2] Therefore, in the distribution system, distribution static compensator (DSTATCOM) is used to compensate the harmonic, reactive and neutral currents.[3-5]

The available DSTATCOM topologies and the design of various parameters of DSTATCOM, such as DC link capacitor, DC link voltage, interfacing inductor are presented in literature.[6-10] Among them, three H-bridge (HB), three-phase split-capacitor (TPSC) and four leg DSTATCOM (FL-DSTATCOM) topologies are mostly used for three-phase four-wire (3P4W) applications.[10] However, three HB topology has the limitation of more switches and also requires isolation transformer for coupling.[2] TPSC topology reduces the requirement of more number of switches, but the capacitor voltage balancing is a nagging issue and also this topology requires higher DC link voltage.[8] Even though, FL-DSTATCOM requires two additional switches compared to TPSC, advantages such as better controllability, low DC link voltage and absence capacitor voltage balancing problem gives priority to FL-DSTATCOM over to other topologies.[2,11-13] Therefore, in this paper a FL-DSTATCOM is used to compensate the current related power quality issues.

Model predictive control (MPC) methods have been gaining the attention of researchers over traditional pulse width modulation and hysteresis-based controllers because of the elegant concept, model-based implementation, elimination of modulating signal, easy addition of control parameters and better attention to added constraints.[14-21] In current control using conventional MPC, the difference between the reference and actual DSTATCOM currents is formed as a cost function (current error) and its value is calculated for each available switching state. Among the available switching states, the state which will minimize the cost function is selected and is applied for the next sampling.[17-19] In FL-DSTATCOM topologies, cost function will also consist the neutral current term along with phase currents, if the output voltage at the each leg of the inverter is measured with respect to the negative DC rail. The additional neutral current term in the cost function will be eliminated, by measuring the inverter voltage with respect to neutral leg.[20] However, the dependency of phase voltage on neutral voltage will further increase the neutral leg switching frequency.[22] As mentioned earlier, the advantage of the MPC is easy addition and better attention to control parameters, the limitation of higher switching frequency can be easily reduced by adding the difference between the present and previous switching state as an additional control parameter using a weighting factor. The tuning of weighting factor during multiple constraint case is a cumbersome process.[23] However, it can be simplified by applying the traditional multi-criteria decision making (MCDM) methods.[24] Therefore, in this paper a MCDM method, namely, the technique for order of preference by similarity to ideal solution (TOPSIS) is used. Using this method, a better alternative among the available switching states is selected based on concepts of compromise solution. The reduction in neutral leg frequency of FL-DSTATCOM will also reduce the phase leg frequency because each is dependent on other.

Conventional operation of DSTATCOM mostly involves two different modes. Between them one is harmonic free (HF) mode and the other is power factor correction (PFC) mode. During balanced and sinusoidal supply voltages, both HF and PFC modes will achieve the similar performance. However, during unbalance and distortions in supply voltage, it is not possible to operate the DSTATCOM in HF and PFC mode simultaneously.[25,26] This is because perfect compensation of harmonics may not provide unity power factor; likewise, unity power factor operation does not guarantee perfect harmonic compensation.[27,28] Therefore, in this paper, only HF operation of FL-DSTATCOM is considered, which will achieve balanced and sinusoidal source currents.

The performance of DSTATCOM mainly depends on reference current extraction and control algorithm that is used to generate gate pulses. A considerable amount of investigations have already been accomplished in the area of reference current extraction techniques.[29-31] Extraction of reference currents is a challenging task when the loads are supplied by unbalanced and distorted voltages, because they depend on upstream loads and voltage unit vectors.[32-34] In general, the

unit vectors of a three-phase balanced system are sinusoidal in nature, and also have unit amplitude.[19,35,36] In most of the control algorithms, the direct estimation of unit vectors from voltages at the point of common coupling (PCC) leads to deviation of unit vectors, during unbalance and distortions in supply voltage.[19,37-39] Therefore, in this paper, a combination of state observer[36,40] and theory of symmetrical components is used to estimate unit vectors, which have the same nature as ideal unit vectors. After extracting unit vectors, conductance factor-based method[19,41] is implemented in which, the extracted unit vectors and load currents detected are used to estimate the reference source currents. Finally, the difference between load currents and reference source currents gives us reference DSTATCOM currents.

Therefore, in this paper,

1. In this paper, MPC of FL-DSTATCOM is proposed to compensate the power quality issues and reduce the neutral leg switching frequency of FL-DSTATCOM during unbalanced and distorted supply conditions.
2. A combination of state observer and theory of symmetrical components is used to extract the reference currents during unbalance and distortion in supply voltages.
3. Difference between the reference and predicted compensator currents is considered as a primary constraint in the cost function and compensation of power quality issues is achieved by selection of a switching state which minimizes this cost function.
4. Higher neutral leg switching frequency of FL-DSTATCOM (considered as a second objective) is reduced by adding an additional constraint to the cost function.
5. Weighting factor selection during multiple constraint case is a challenging task and in the proposed work TOPSIS method is used to achieve the simplification of weighting factor selection.

The proposed work is organized as follows. Section 2 explains the configuration and predictive model of FL-DSTATCOM, cost function formation, simplification of weighting factor tuning using TOPSIS method and improved conductance factor-based control algorithm for reference current extraction. Sections 3 and 4 validate the performance of the proposed method using simulation and experimental results. Finally, Section 5 summarizes the complete work.

2 | PROPOSED TOPSIS-BASED MPC FOR FL-DSTATCOM

Schematic diagram of the FL-DSTATCOM is shown in Figure 1. FL-DSTATCOM is connected at PCC through the interfacing inductor which eliminates the switching harmonics in compensating current. PCC voltages (v_{sabc}), load

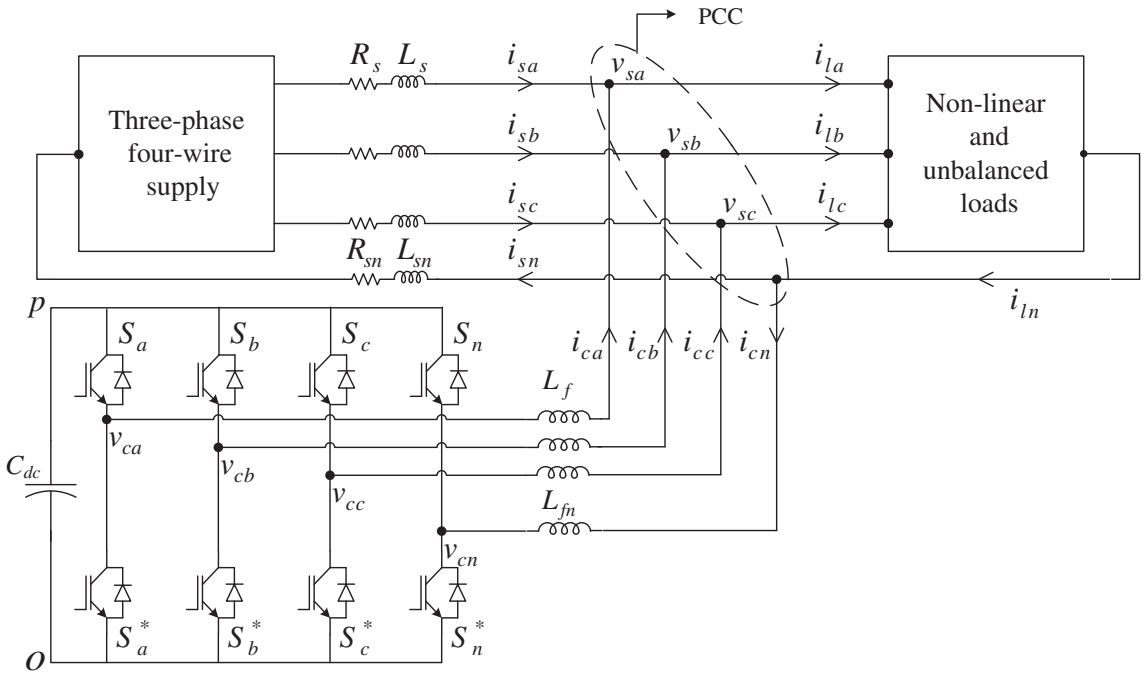

FIGURE 1 Schematic diagram of a FL-DSTATCOM connected distribution system

currents (i_{labc}), DSTATCOM currents (i_{cabc}) and DC link voltage (V_{dc}) are detected to implement the proposed control algorithm. The step by step procedure of the proposed control algorithm is explained as follows.

2.1 | FL-DSTATCOM predictive model and formation of cost function

FL-DSTATCOM has 16 possible switching states. The value of pole voltage for an individual phase is V_{dc}, if the upper switch of a leg is turned on, while it is zero, if the lower switch is turned on. The model of the FL-DSTATCOM is used to predict the DSTATCOM currents. From Figure 1, the sum of voltage drop across the interfacing inductor and voltage at the PCC is equal to the output voltage of inverter which can be written as follows,

$$v_{ca} = L_f \frac{\mathrm{d}i_c}{\mathrm{d}t} + R_f i_c + v_{sa} \tag{1}$$

where,

$$v_c = [v_{can}\ v_{cbn}\ v_{ccn}]^T, i_c = [i_{ca}\ \ i_{cb}\ \ i_{cc}]^T, \text{and } v_s = [v_{sa}\ \ v_{sb}\ \ v_{sc}]^T.$$

Solve (1) for $\frac{\mathrm{d}i_c}{\mathrm{d}t}$,

$$\frac{\mathrm{d}i_c}{\mathrm{d}t} = \frac{(v_c - v_s)}{L_f} - \frac{i_c R_f}{L_f}. \tag{2}$$

Forward Euler approximation method[14] is used to simplify (2), and according to this method,

$$\frac{\mathrm{d}i_c}{\mathrm{d}t} = \frac{i_c(k+1) - i_c(k)}{T_s}. \tag{3}$$

Substitute (3) in (2) and simplify (2) for $i_c(k+1)$

$$i_c(k+1) = \frac{(v_c(k) - v_s(k))T_s}{L_f} + i_c(k)\left(1 - \frac{R_f T_s}{L_f}\right). \tag{4}$$

From (4), it is observed that the predicted value of DSTATCOM current ($i_c(k+1)$) depends on filter current ($i_c(k)$), inverter output voltage ($v_c(k)$) and PCC voltage at kth instant ($v_s(k)$). Compensation of current related power quality issues using conventional MPC involves the minimization of the difference between the reference and predicted value of DSTATCOM current.[18-21]

$$C_1 = |\, i_c^*(k+1) - i_c(k+1)\,|. \tag{5}$$

In the above equation, $i_c^*(k+1)$ represents the reference DSTATCOM current and they are extracted using an improved conductance factor-based control algorithm, which is explained in the Section 2.3. As mentioned earlier, to limit the higher neutral leg switching frequency of FL-DSTATCOM, it is required to consider the difference between the present and previous switching state of the neutral leg as an additional constraint, which is given by,

$$C_2 = |\, S_n(k) - S_n(k-1)\,|. \tag{6}$$

A single cost function for current control and switching frequency reduction is formed by adding two individual cost functions (C_1, C_2) using a weighting factor (λ).

$$C = C_1 + \lambda C_2. \tag{7}$$

where, the value of λ ranges from $(0 - \infty)$. The compensation using MPC depends upon λ and there is no particular method present to find the value of λ.[23] However, the traditional MCDM methods simplify the weighting factor tuning

by reducing the range from $(0 - \infty)$ to (0-1). Therefore, in the proposed work, simplification of weighting factor selection is done using a MCDM method namely TOPSIS. In this method, the best alternative from the available options is selected, which should be closer to the negative ideal solution and far away from the positive ideal solution.

2.2 | Weighting factor simplification and cost function minimization using TOPSIS-based MPC

The flowchart of the switching state selection using TOPSIS method is shown in Figure 2. The detailed procedure of weighting factor tuning simplification and selection of suitable switching state using TOPSIS method is explained as follows.

Step 1: Initially, individual cost functions (C_1, C_2) are evaluated using (5) and (6) for all the possible switching states of FL-DSTATCOM and they are represented as:

$$C_{PQ} = \begin{bmatrix} C_{11} & C_{12} \\ C_{21} & C_{22} \\ \vdots & \vdots \\ C_{p1} & C_{p2} \end{bmatrix}_{pq} \tag{8}$$

where, "p" indicates the number of switching states (16 switching states) and "q" indicates the number of individual cost functions (two cost functions).

Step 2: Select the switching states of each cost function, which have minimum and maximum cost function values and they are represented as,

$$\begin{aligned} C_{m1} &= \min(C_{i1}), C_{M1} = \max(C_{i1}); \\ C_{m2} &= \min(C_{i2}), C_{M2} = \max(C_{i2}). \end{aligned} \tag{9}$$

where "i" varies from 1 to "p".

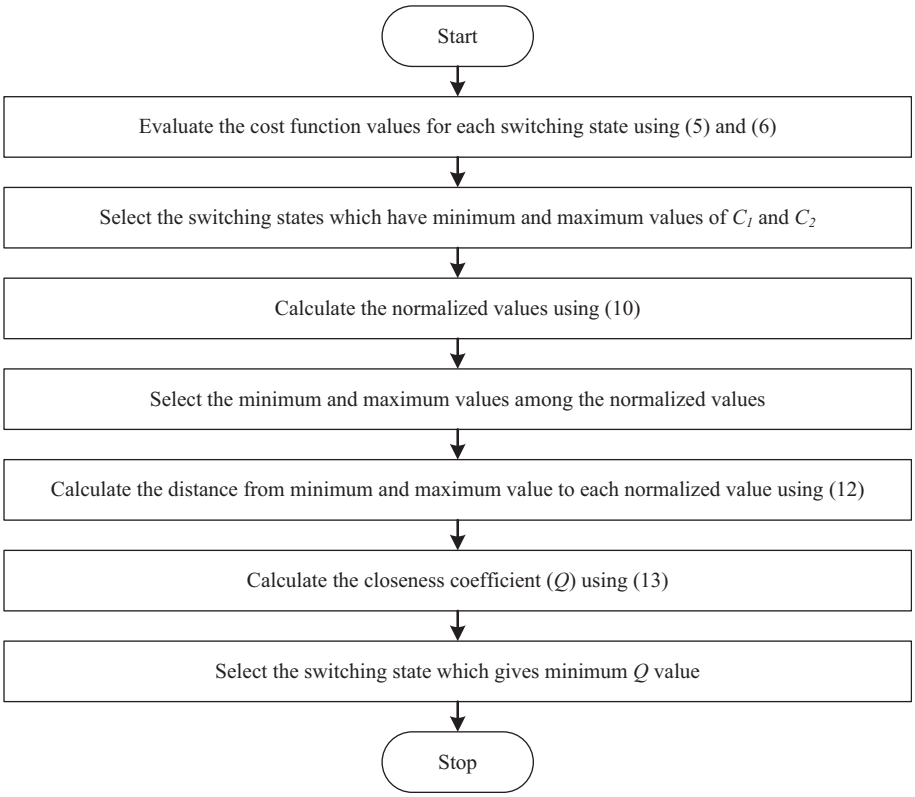

FIGURE 2 Switching state selection using TOPSIS method

Step 3: Calculation of normalized data from the obtained values from step 1 and step 2, using the following formula.

$$X_{i1} = \sigma_1 \left(\frac{C_{m1} - C_{i1}}{C_{m1} - C_{M1}} \right); \\ X_{i2} = \sigma_2 \left(\frac{C_{m2} - C_{i2}}{C_{m2} - C_{M2}} \right). \tag{10}$$

The values σ_1 and σ_2 depend on the importance between the two individual cost functions and the sum of σ_1 and σ_2 should always be equal to unity. In the proposed work, the primary objective is current control and the other objective is switching frequency reduction. Therefore, the value of σ_1 is chosen as 0.8 and the value of σ_2 is chosen as 0.2.

Step 4: Select the positive and negative best values from the normalized data which is obtained from step 3.

$$X_{m1} = \min(X_{i1}), X_{M1} = \max(X_{i1}); \\ X_{m2} = \min(X_{i2}), X_{M2} = \max(X_{i2}) \tag{11}$$

where, X_{m1}, X_{m2} are the negative best values and X_{M1}, X_{M2} are the positive best values.

Step 5: After finding the positive and negative best values from the normalized data, calculate the distance of each value from positive (D_i^+) and negative best values (D_i^-).

$$D_i^+ = \sqrt{(X_{i1} - X_{M1})^2 + (X_{i2} - X_{M2})^2}; \\ D_i^- = \sqrt{(X_{i1} - X_{m1})^2 + (X_{i2} - X_{m2})^2}. \tag{12}$$

Step 6: In this step closeness coefficient (Q) to the negative ideal solution is calculated, because the switching state which is giving the minimum error should be applied at the next instant.

$$Q = \frac{D_i^-}{D_i^+ + D_i^-} \tag{13}$$

Step 7: In the last step, the state for which the value of Q is minimum is selected and is applied to FL-DSTATCOM for compensation current-related power quality issues along with switching frequency reduction of neutral leg. In this paper, minimization of current error (C_1) alone is considered as conventional method.[21] Application of TOPSIS method to minimize the current error (C_1) along with switching frequency reduction (C_2) is considered as the proposed method.

2.3 | Extraction of reference currents with improved conductance factor method

In this paper, conventional conductance factor-based reference current extraction method[19,41] is improved to adapt it for unbalanced and distorted supply voltages. According to the conventional method, the amplitude of fundamental active component of load current (I_{lpma}, I_{lpmb} and I_{lpmc}) is equal to conductance factor (G_a, G_b and G_c) and it is given by,

$$I_{lpma} = G_a(t) = \sum_{j=1}^{N} \left(i_{laj} - i_{la(j-1)} \right) \left(u_{qaj} \times K_1 + u_{paj} \times K_2 \right); \\ I_{lpmb} = G_b(t) = \sum_{j=1}^{N} \left(i_{lbj} - i_{lb(j-1)} \right) \left(u_{qbj} \times K_1 + u_{pbj} \times K_2 \right); \\ I_{lpmc} = G_c(t) = \sum_{j=1}^{N} \left(i_{lcj} - i_{lc(j-1)} \right) \left(u_{qcj} \times K_1 + u_{pcj} \times K_2 \right) \tag{14}$$

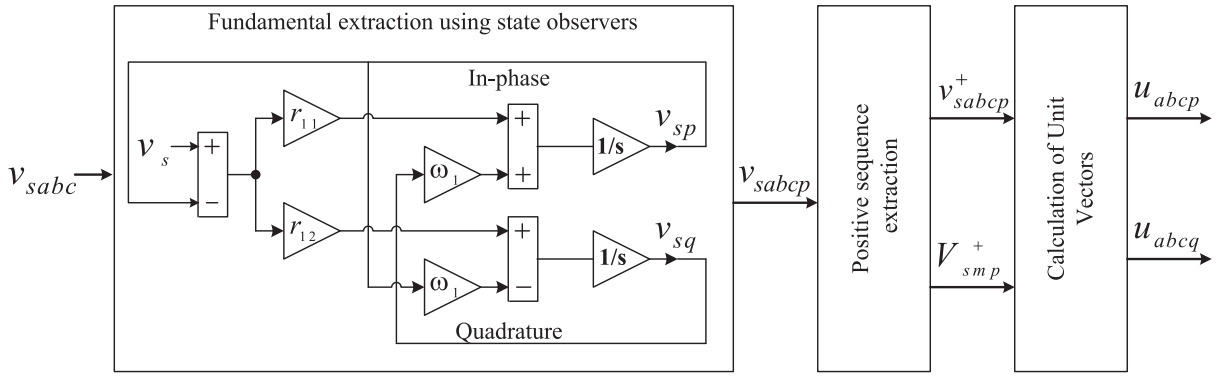

FIGURE 3 Extraction of unit vectors using state observer and theory of symmetrical components

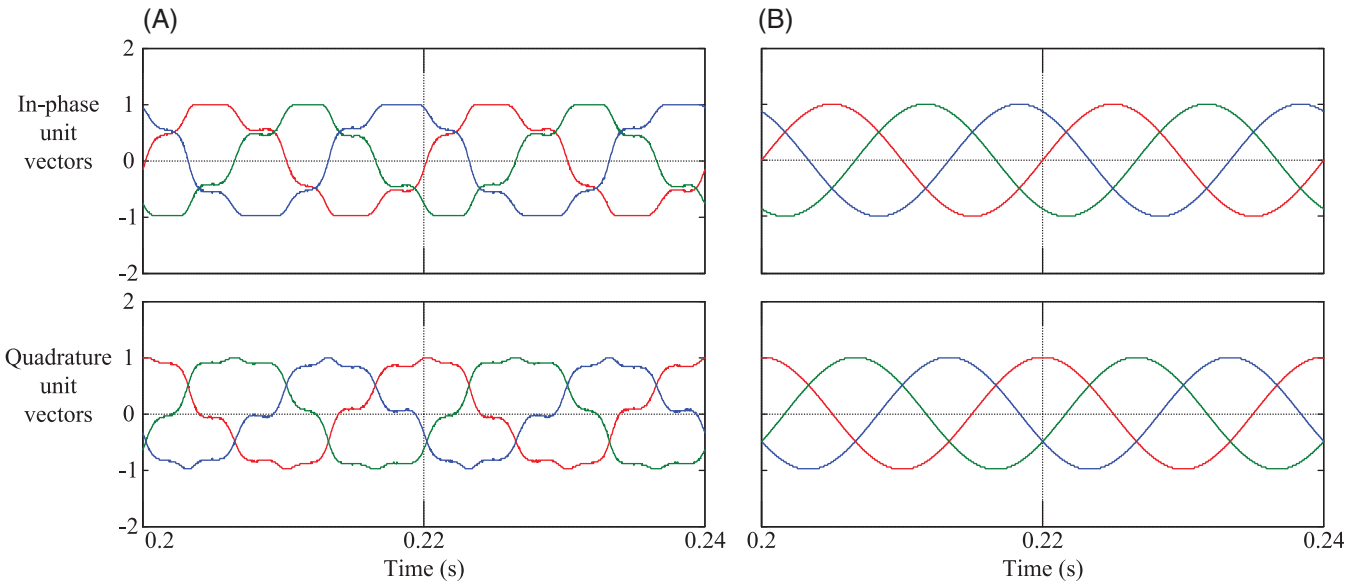

FIGURE 4 Unit vectors using (A) Conductance factor method,[19,41] and (B) Improved conductance factor method

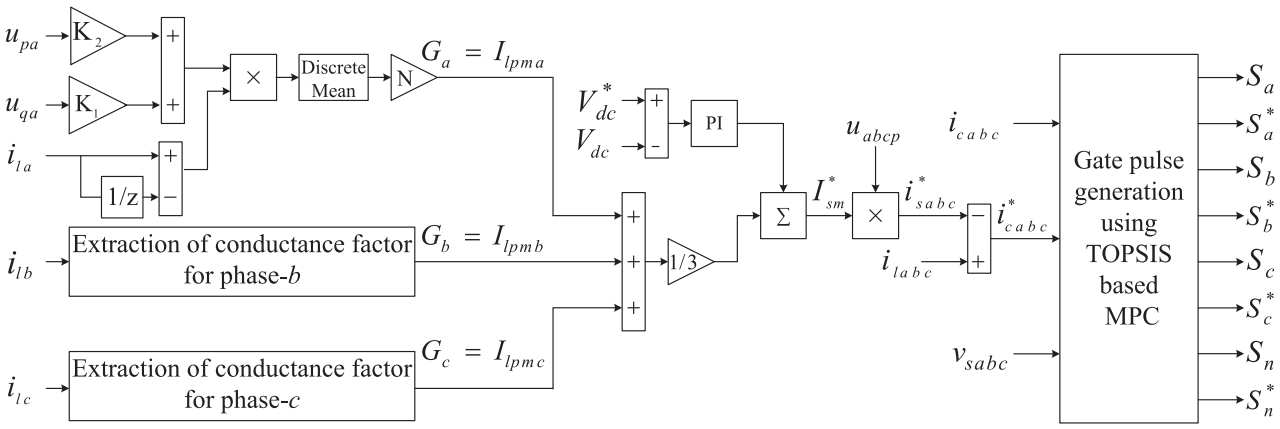

FIGURE 5 Proposed conductance factor-based control algorithm for FL-DSTATCOM

TABLE 1 Simulation parameters

Parameters	Values
Unbalanced and distorted	$V_{sa1} = 240$ V; $V_{sb1} = 0.8 \times 240$ V; $V_{sc1} = 1.2 \times 240$ V.
Supply voltage	$V_{sa5} = 0.2 \times 240$ V; $V_{sb5} = 0.24 \times 240$ V; $V_{sc5} = 0.16 \times 240$ V.
Feeder impedance (Z_S)	0.07 Ω, 0.2 mH
Interfacing inductor (L_f)	5 mH
Neutral impedance (Z_{Sn})	0.07 Ω, 2 mH
DC link (V_{dc}, C_{dc})	700 V, 5000 μF
Sampling time (T_s)	10 μs
Load	Case-1
	(a) Three phase diode bridge rectifier feeding an *RL* load with $R = 12$ Ω, $L = 50$ mH on phase
	(b) Unbalanced linear load with $R_a = 5$ Ω, $L_a = 50$ mH (on phase-*a*) and
	$R_b = 10$ Ω, $L_b = 50$ mH (on phase-*b*)
	Case-2
	(a) Three-single phase diode bridge rectifiers feeding $R = 5$ Ω, $L = 150$ mH (on phase-*a*),
	$R = 7$ Ω, $L = 150$ mH (on phase-*b*) and $R = 6$ Ω, $L = 150$ mH (on phase-*c*).
	(b) Balanced linear load with $R = 15$ Ω, $L = 30$ mH.

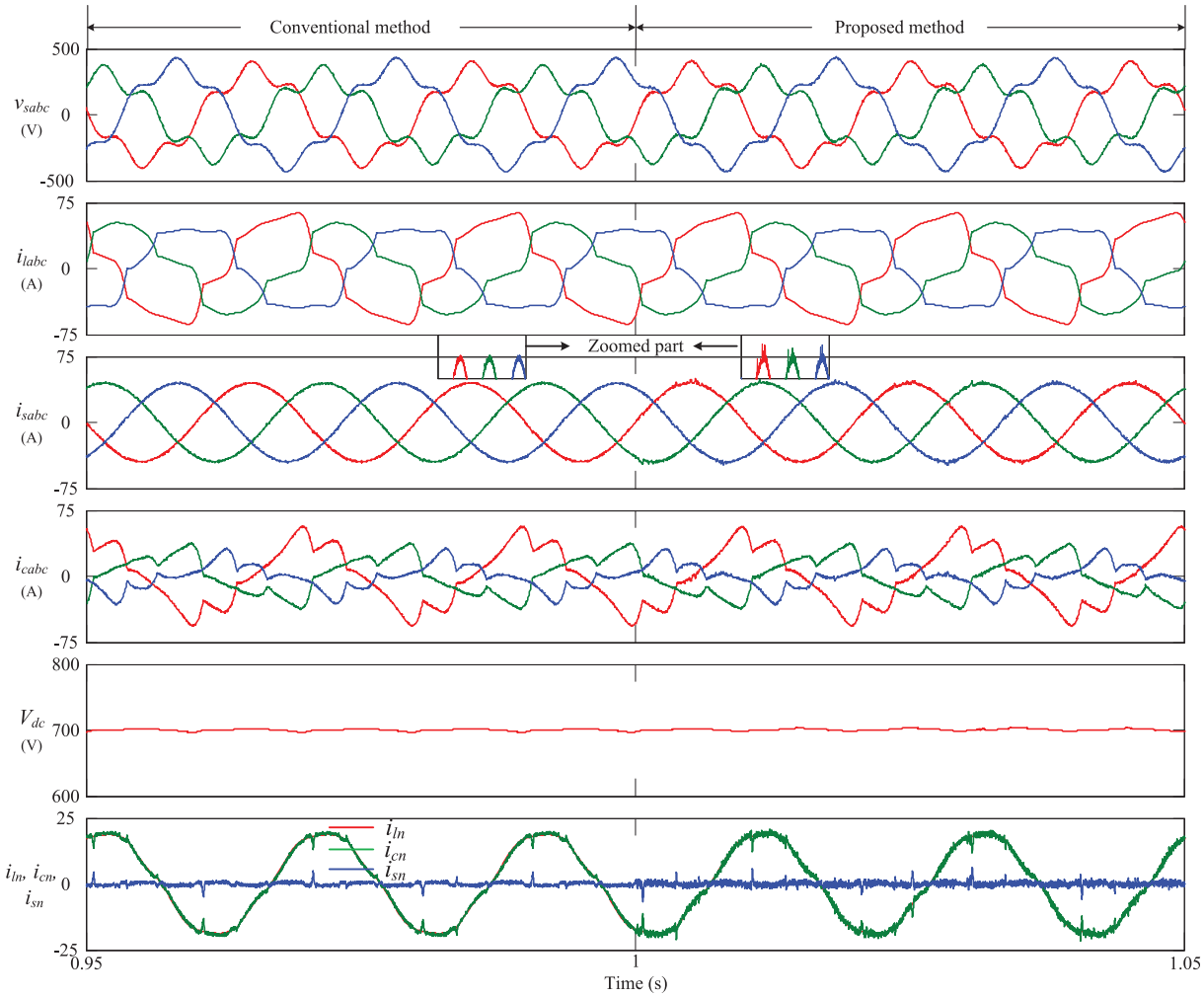

FIGURE 6 Voltages and currents during case-1

where, K_1 and K_2 are constants and they are given by $K_1 = \frac{\cos(\omega T_s/2)}{N\sin(\omega T_s/2)}$, $K_2 = \frac{1}{N}$, and N is the ratio of fundamental time period (0.02 second) to the sampling time (T_s). In (14), u_{pa}, u_{pb} and u_{pc} represent the in-phase unit vectors and quadrature unit vectors are represented as u_{qa}, u_{qb} and u_{qc}. From (14), it is observed that, the estimation of conductance factors or amplitude of reference source currents mainly depends mainly on load currents and unit vectors extracted from PCC voltages. During balanced and sinusoidal supply voltages, in-phase unit vectors are expressed as,[4,19,36]

$$u_{pa} = \frac{v_{sa}}{V_{sm}}; u_{pb} = \frac{v_{sb}}{V_{sm}}; u_{pc} = \frac{v_{sc}}{V_{sm}} \tag{15}$$

where, v_{sa}, v_{sb}, and v_{sc} represent the phase voltages and V_{sm} represents the peak amplitude of PCC voltage and it is given by:

$$V_{sm} = \sqrt{\frac{2}{3}\left(v_{sa}^2 + v_{sb}^2 + v_{sc}^2\right)}. \tag{16}$$

Correspondingly, the quadrature unit vectors are expressed as[4,19,36]:

$$u_{qa} = \frac{-u_{pb} + u_{pc}}{\sqrt{3}}; u_{qb} = \frac{3u_{pa} + u_{pb} - u_{pc}}{2\sqrt{3}}; u_{qc} = \frac{-3u_{pa} + u_{pb} - u_{pc}}{2\sqrt{3}}. \tag{17}$$

In general, the magnitude of unit vector is 1 and they should be HF. However, during unbalance and distortion in supply voltages, the unequal amplitudes and the presence of distortion in PCC voltages, makes it difficult to estimate unit vectors using (15) and (17). The extraction of unit vectors from fundamental positive sequence voltages eliminates this difficulty, because the fundamental positive sequence voltages are equal in amplitude and distortion free. The extraction of fundamental in-phase and quadrature voltages from a voltage signal using state observer is shown in Figure 3.[36,40]

State equation and output equations are represented as:

$$\begin{aligned} \dot{v}_s(t) &= A v_s(t) \\ v(t) &= C^T v_s(t) \end{aligned} \tag{18}$$

where, $v_s = \begin{bmatrix} v_{sp}(t) \\ v_{sq}(t) \end{bmatrix}, A = \begin{bmatrix} 0 & \omega_1 \\ -\omega_1 & 0 \end{bmatrix}, C^T = [1 \;\; 0]$, $v(t)$ is the desired output voltage, $v_{sp}(t)$ and $v_{sq}(t)$ are fundamental in-phase and quadrature voltages. In closed loop system, the observation error is given as,[36,40]

TABLE 2 Comparison of the proposed TOPSIS-based MPC with conventional and VIKOR-based MPC methods

Parameters	Conventional MPC	MPC with VIKOR method	MPC with TOPSIS method
v_{sa} (V, THD)	239.3 (20.33%)	239.3 (20.33%)	239.2 (20.31%)
v_{sb} (V, THD)	213.8 (24.90%)	213.8 (24.90%)	213.8.2 (24.87%)
v_{sc} (V, THD)	261.6 (16.64%)	261.6 (16.64%)	261.6 (16.63%)
i_{la} (A, THD)	43.16 (16.11%)	43.16 (16.11%)	43.16 (16.11%)
i_{lb} (A, THD)	34.65 (22.81%)	34.65 (22.81%)	34.66 (22.81%)
i_{lc} (A, THD)	35.38 (17.35%)	35.38 (17.35%)	35.38 (17.34%)
i_{sa} (A, THD)	31.69 (1.68%)	31.68 (2.63%)	31.74 (2.68%)
i_{sb} (A, THD)	31.74 (1.81%)	31.67 (2.01%)	31.53 (2.08%)
i_{sc} (A, THD)	31.65 (1.48%)	31.68 (2.14%)	31.7 (2.25%)
S_a	20 765 Hz	15 385 Hz	14 841 Hz
S_b	22 695 Hz	15 734 Hz	14 561 Hz
S_c	19 317 Hz	15 130 Hz	13 333 Hz
S_n	29 690 Hz	13 037 Hz	11 039 Hz

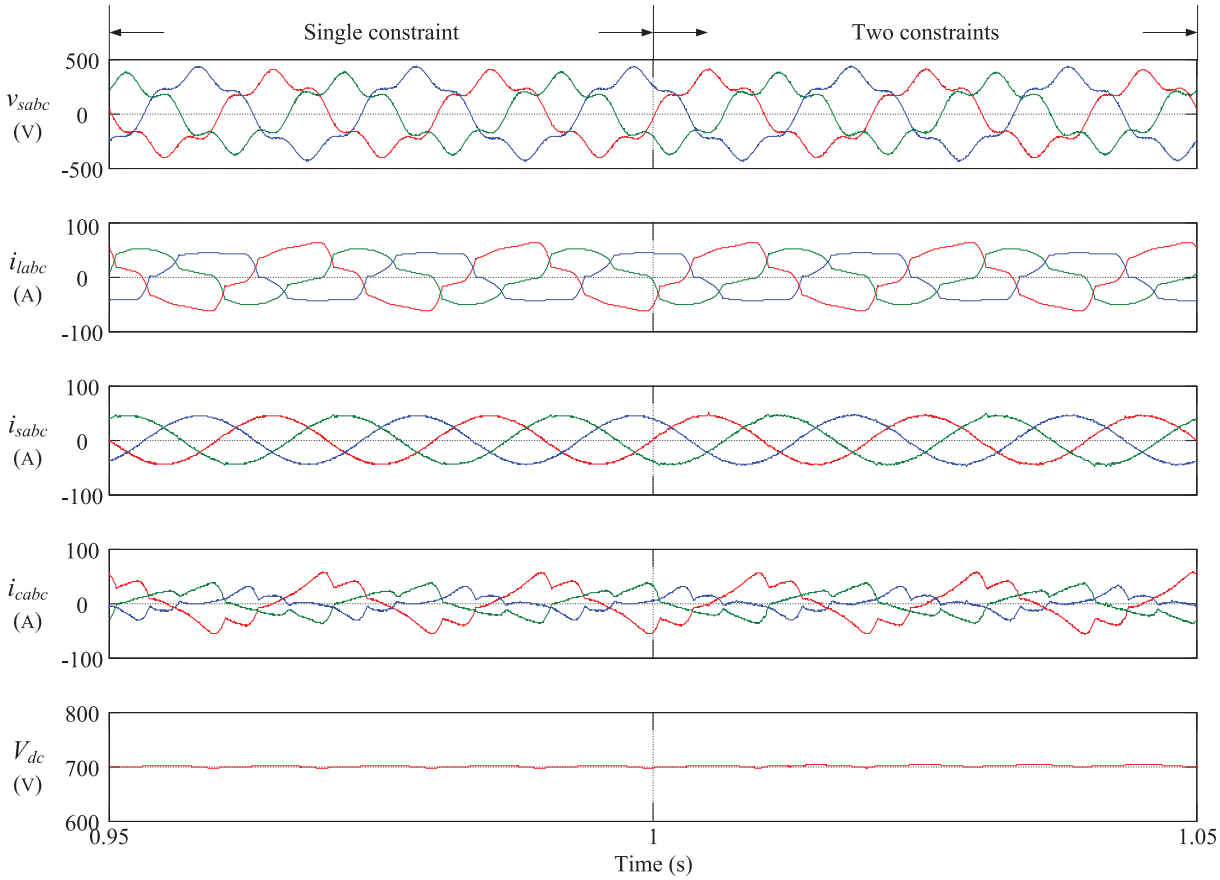

FIGURE 7 Performance of FL-DSTATCOM with VIKOR method

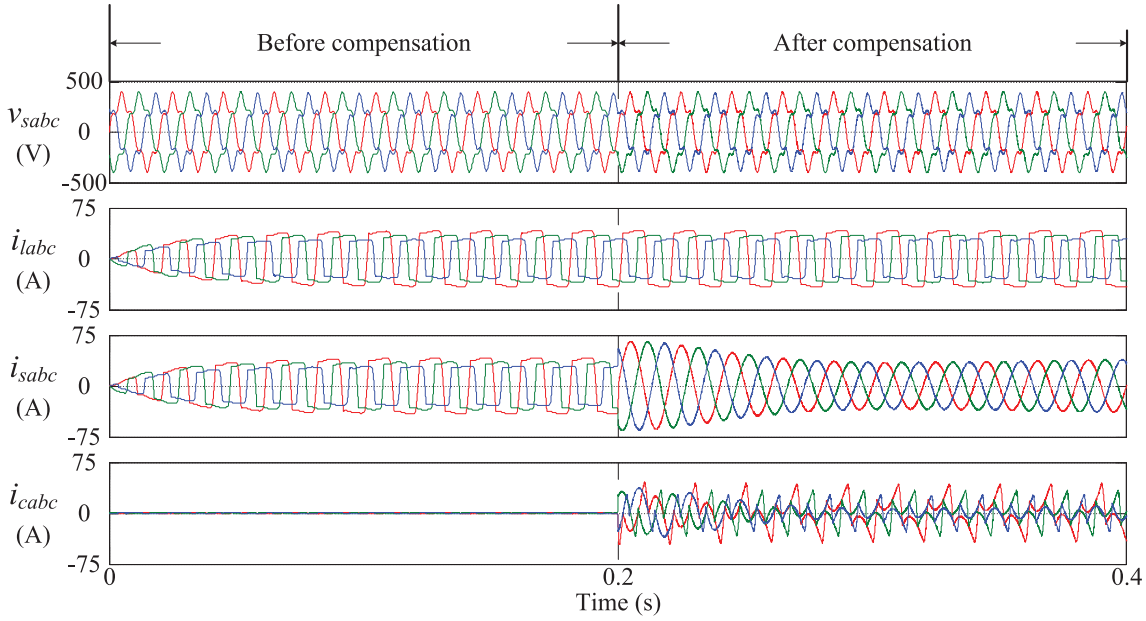

FIGURE 8 Voltages and currents before and after connecting FL-DSTATCOM

$$e(t) = v(t) - \hat{v}(t). \tag{19}$$

Then the model of the observer becomes

$$\begin{aligned} \dot{\hat{v}}_s(t) &= A\hat{v}_s(t) + Re(t); \\ \hat{v}(t) &= C^T\hat{v}_s(t) \end{aligned} \tag{20}$$

where $R = [r_{11} \quad r_{12}]^T$. The state error vector can be written as

$$\dot{v}_s(t) - \dot{\hat{v}}_s(t) = Av_s(t) - A\hat{v}_s(t) - Re(t) = \left(A - RC^T\right)(v_s(t) - \hat{v}_s(t)). \tag{21}$$

The above equation can also be written as

$$\dot{e}(t) = \left(A - RC^T\right)e(t). \tag{22}$$

The characteristic equation of error will be

$$|SI - \left(A - RC^T\right)| = 0 \tag{23}$$

The roots of the error characteristic equation are the closed loop poles. The value of R can be chosen such that, $(A - RC^T)$ has reasonably fast and stable roots.[36,40] The assumed closed loop poles are

$$S = (-a\omega \pm j\omega) \tag{24}$$

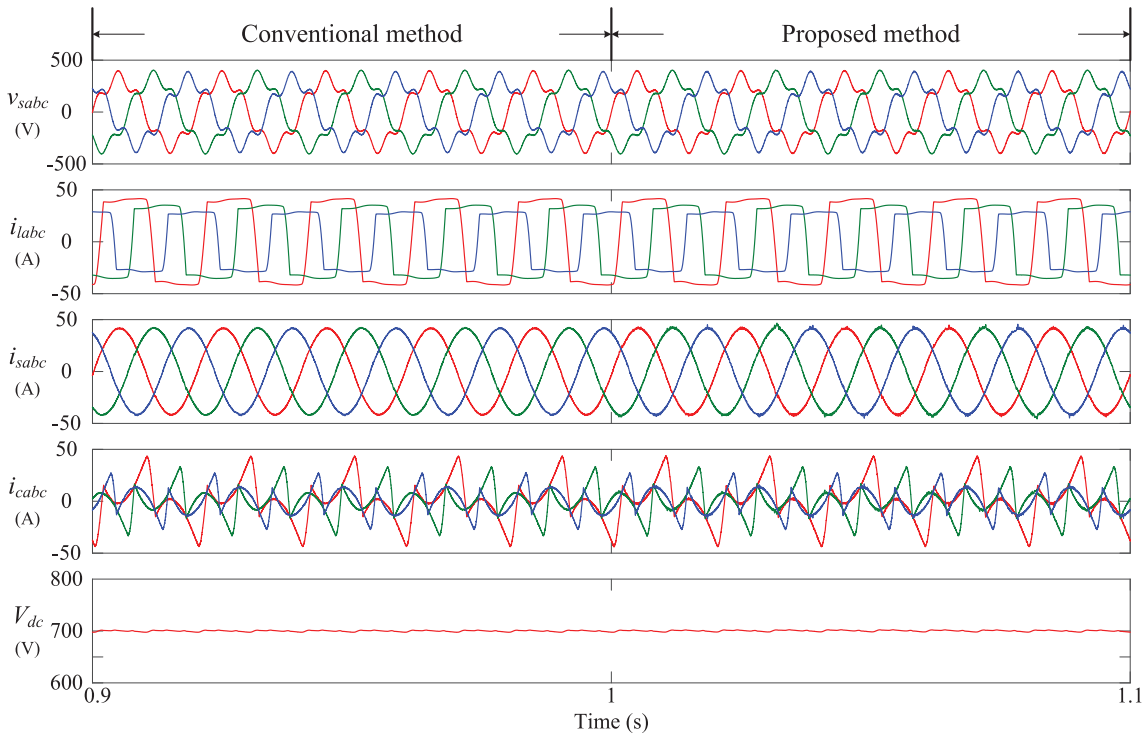

FIGURE 9 Voltage and currents during case-2

Parameters	Conventional (0 to 1) s	Proposed (1 to 2) s
v_{sa} (THD)	239.3 V (20.79%)	239.2 V (20.31%)
v_{sb} (THD)	213.8 V (24.84%)	213.8 V (24.87%)
v_{sc} (THD)	261.7 V (16.62%)	261.6 V (16.63%)
i_{la} (THD)	35.96 A (34.86%)	35.96 A (34.86%)
i_{lb} (THD)	30.5 A (37.33%)	30.5 A (37.33%)
i_{lc} (THD)	25.1 A (38.70%)	25.1 A (38.70%)
i_{sa} (THD)	29.61 A (1.75%)	29.64 A (2.15%)
i_{sb} (THD)	29.63 A (1.80%)	29.69 A (2.14%)
i_{sc} (THD)	29.5 A (1.78%)	29.49 A (2.14%)
S_a	21 992 Hz	17 908 Hz
S_b	21 561 Hz	17 378 Hz
S_c	21 963 Hz	15 380 Hz
S_n	27 752 Hz	10 108 Hz

TABLE 3 Parameters during case-2

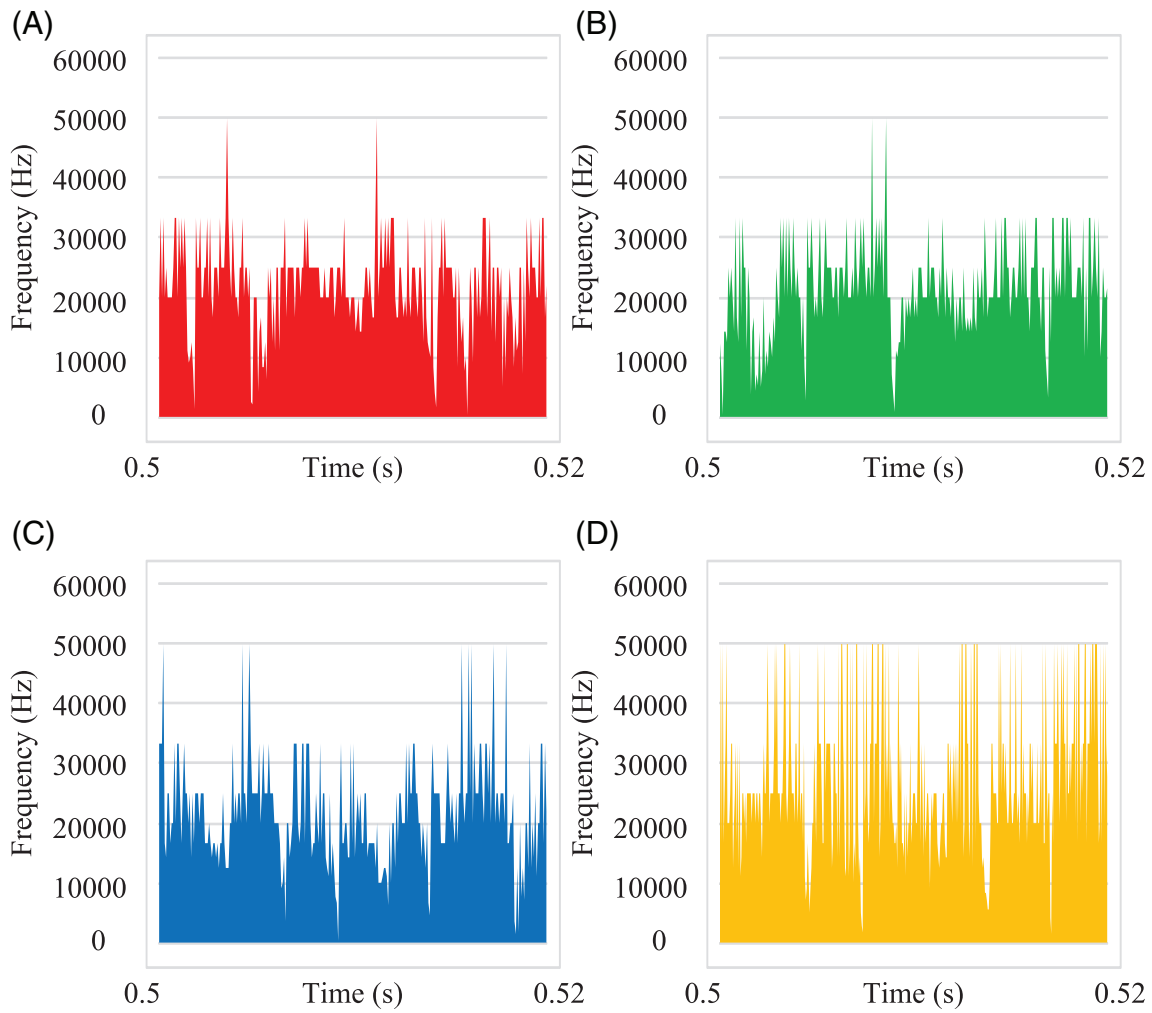

FIGURE 10 Switching frequency with conventional method for (A) Phase-*a* (B) Phase-*b* (C) Phase-*c*, and (D) Neutral leg

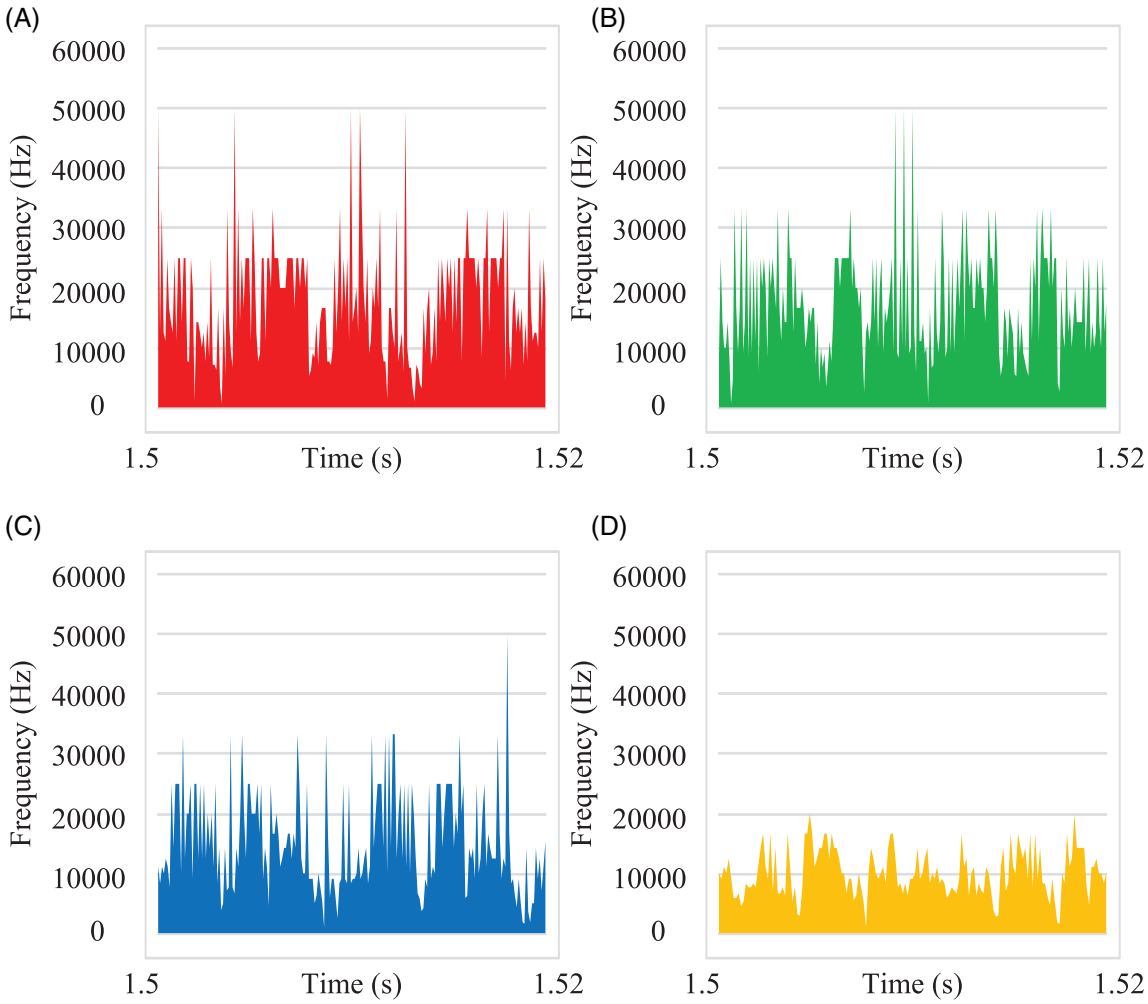

FIGURE 11 Switching frequency with proposed method for (A) Phase-*a* (B) Phase-*b* (C) Phase-*c*, and (D) Neutral leg

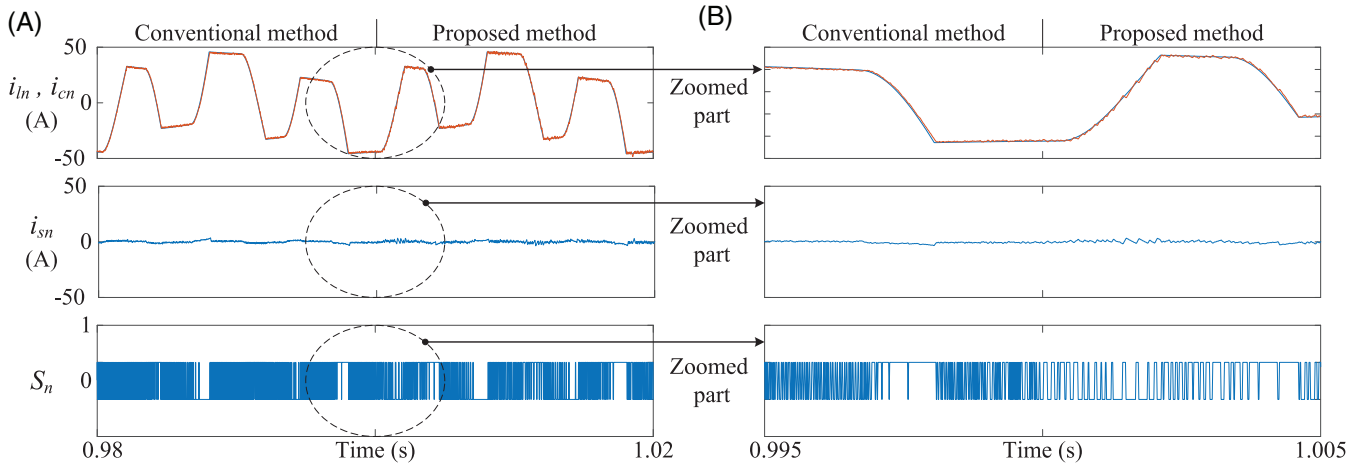

FIGURE 12 Neutral currents during case-2 (A) Conventional method, and (B) Proposed method

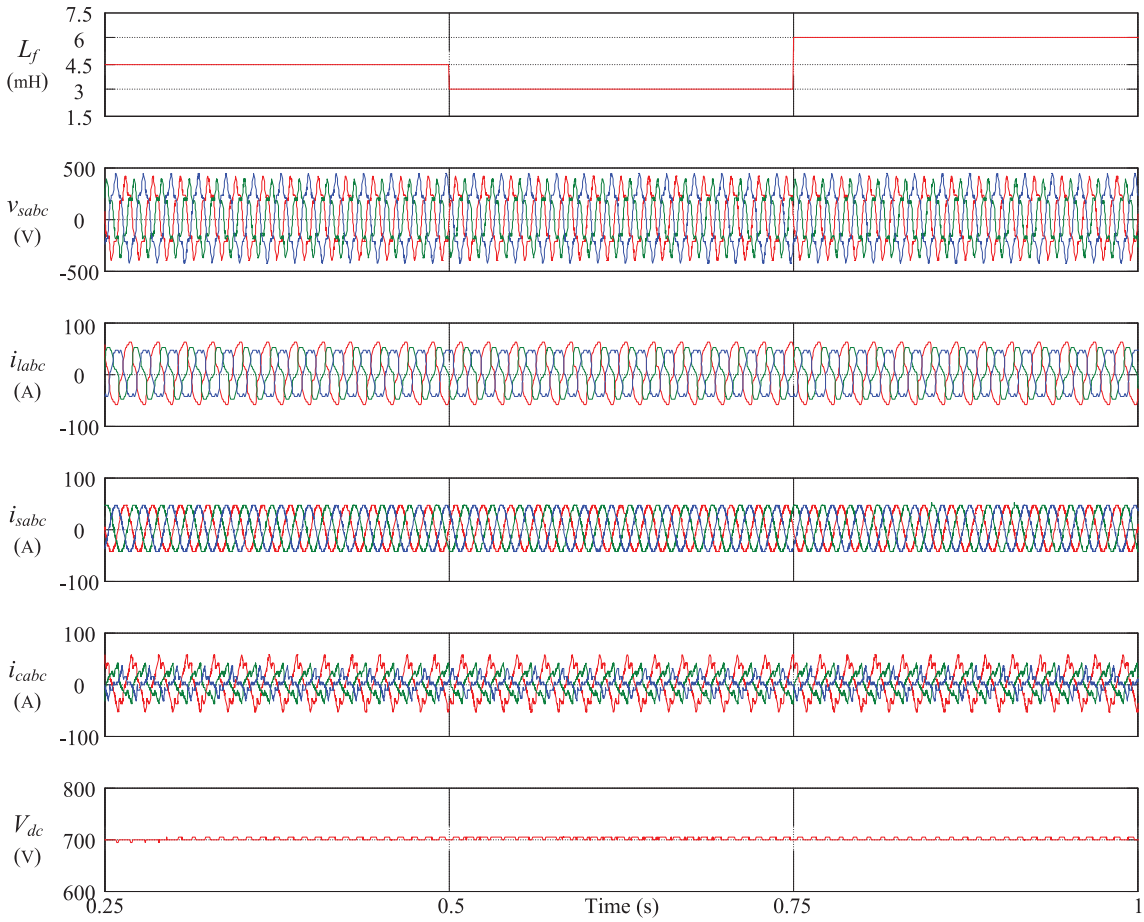

FIGURE 13 Performance during $\sigma_1 = 1$ and $\sigma_2 = 0$ (Case a)

The relation between R and a is

$$R = [r_{11} \;\; r_{12}]^T = [2a\omega \;\; a^2\omega]^T. \tag{25}$$

The transient response of the observer will be decided by the real part of the pole. If the location of the pole is closer to the origin, time constant will be high and output purely sinusoidal. If it is far away from the origin, the time constant is reduced and harmonics will be added to the output signal. Therefore in this paper, the value of a is assumed to be 0.1, so that the obtained values of r_{11} and r_{12} are 62.8 and 3.14, which will provide in-phase and quadrature voltages (v_{sp}, v_{sq}) with better quality. Three state observers are required for the extraction of fundamental voltages from three phases and the same values of r_{11} and r_{12} are applied for all the state observers. State observers are sufficient to extract the unit vectors during distorted supply conditions. But during unbalance and distortions in the supply voltage, amplitudes of each state observer output are different; therefore it is not possible to get unit vectors using only state observers. To overcome this limitation, fundamental positive sequence voltages (v^+_{sabcp}) are required, which have equal amplitude without any distortion. These fundamental positive sequence voltages are extracted using the theory of symmetrical components and they are given by:

$$\begin{bmatrix} v^+_{sap} \\ v^+_{sbp} \\ v^+_{scp} \end{bmatrix} = \frac{1}{3} \begin{bmatrix} 1 & a & a^2 \\ a^2 & 1 & a \\ a & a^2 & 1 \end{bmatrix} \begin{bmatrix} v_{sap} \\ v_{sbp} \\ v_{scp} \end{bmatrix} \tag{26}$$

where, v_{sap}, v_{sbp} and v_{scp} are fundamental in-phase voltages and $a = 1 \angle 120^\circ$. After extracting fundamental positive sequence voltages, they are divided with their amplitudes to get the required in-phase unit vectors and these are given as

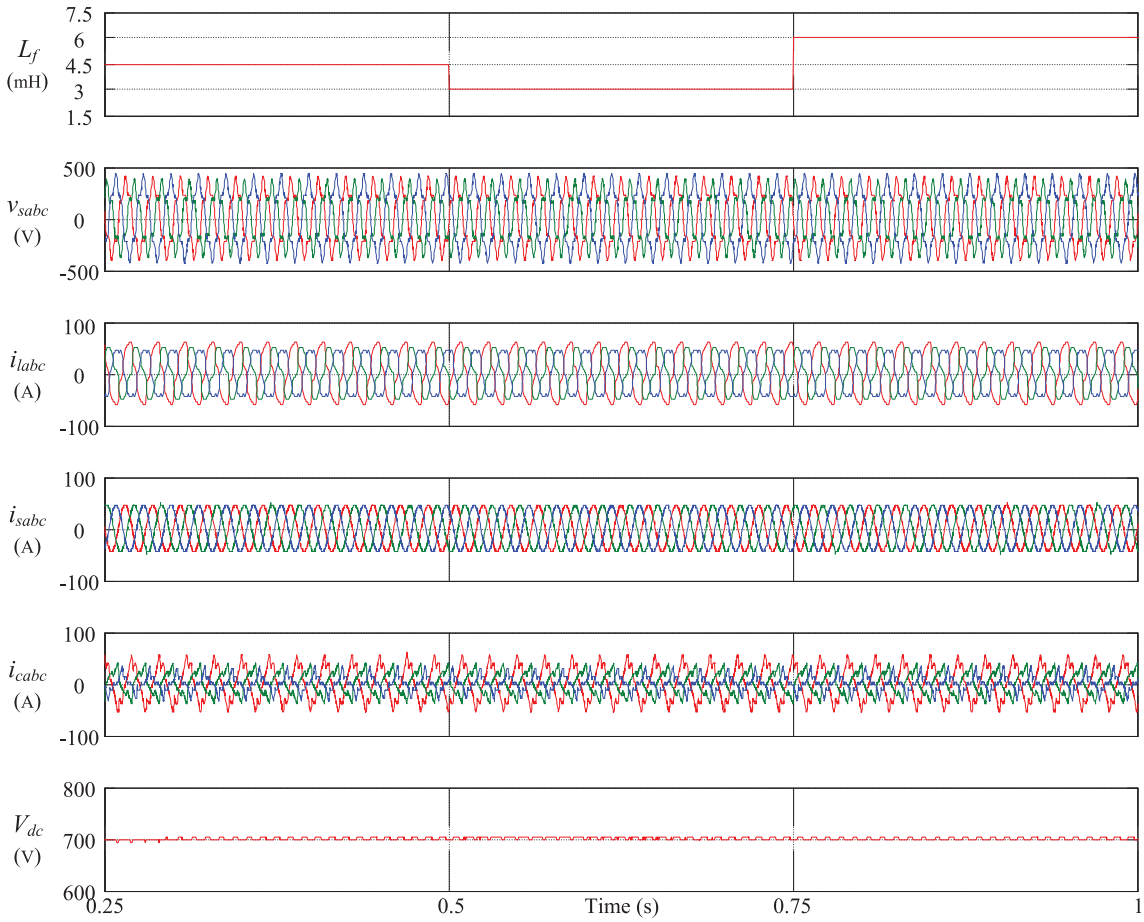

FIGURE 14 Performance during $\sigma_1 = 0.9$ and $\sigma_2 = 0.1$ (Case b)

$$u_{pa} = \frac{v_{sap}^{+}}{V_{smp}^{+}}, u_{pb} = \frac{v_{sbp}^{+}}{V_{smp}^{+}}, u_{pc} = \frac{v_{scp}^{+}}{V_{smp}^{+}} \tag{27}$$

where, the peak amplitude of in-phase voltages is given as $V_{smp}^{+} = \sqrt{\frac{2}{3}\left(\left(v_{sap}^{+}\right)^2 + \left(v_{sbp}^{+}\right)^2 + \left(v_{scp}^{+}\right)^2\right)}$. Quadrature unit vectors are calculated from in-phase unit vectors and they are given as

$$u_{qa} = \frac{-u_{pb} + u_{pc}}{\sqrt{3}}; u_{qb} = \frac{3u_{pa} + u_{pb} - u_{pc}}{2\sqrt{3}}; u_{qc} = \frac{-3u_{pa} + u_{pb} - u_{pc}}{2\sqrt{3}}. \tag{28}$$

Unit vectors extracted using conventional and improved conductance factor method are shown in Figure 4. From this figure, it is observed that, the unit vectors extracted using conventional method are distorted. However, the improved conductance factor method eliminated the difficulty in the unit vector extraction.

The block diagram of improved conductance factor-based reference current extraction and switching pulse generation using MPC is shown in Figure 5. After extracting the fundamental active components of load currents, reference source currents are considered as the average of fundamental active component (I_{lpm}) of three load currents to achieve source currents balanced and sinusoidal, and it is given as,

$$I_{lpm} = \frac{I_{lpma} + I_{lpmb} + I_{lpmc}}{3}. \tag{29}$$

At the same time, DSTATCOMs require active power to support the switching losses of the voltage source inverter. In general, this active power has to be supplied by the utility. The difference between actual and measured DC link

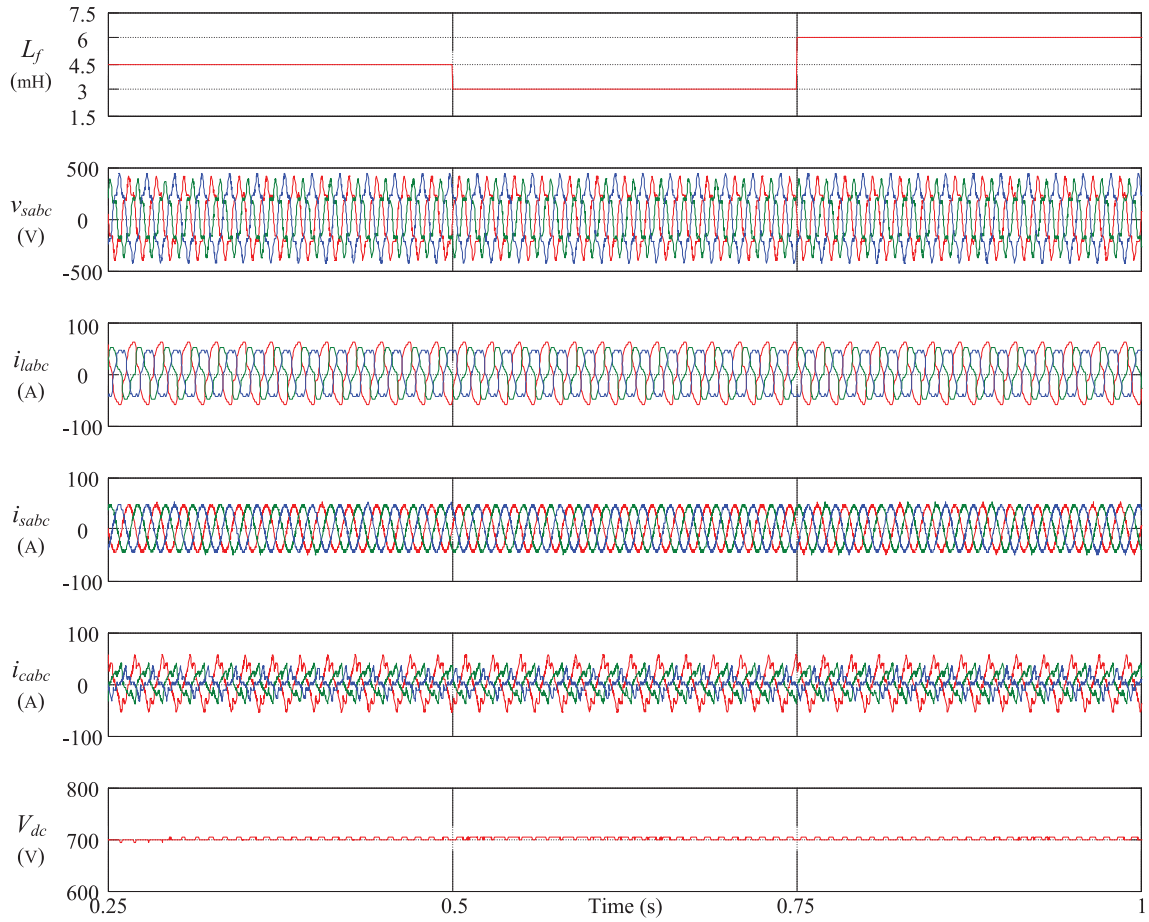

FIGURE 15 Performance during $\sigma_1 = 0.8$ and $\sigma_2 = 0.2$ (Case c)

voltage values $(V_{dc}^* - V_{dc})$ is passed through a PI controller which is generating the required active component of current (I_{dc}^*) and it is responsible for inverter switching losses.

$$I_{dc}^* = K_p\left(V_{dc}^* - V_{dc}\right) + K_i \int \left(V_{dc}^* - V_{dc}\right) \mathrm{d}t. \tag{30}$$

Ziegler-Nichols method[42] is used to select the values of K_p and K_i. In the above equation the value of K_p is considered as 0.45 and the value of K_i is considered as 4.5. The amplitude of reference source current is obtained by adding average value of fundamental active component of load current and the current required for maintaining constant voltage across the DC link $(I_{sm}^* = I_{lpm} + I_{dc}^*)$. After getting the amplitude (I_{sm}^*), it is multiplied with the respective unit vectors in (27) to obtain the reference source currents of phase-a, phase-b and phase-c and they are given in (31).

$$i_{sa}^* = I_{sm}^* \times u_{pa}, i_{sb}^* = I_{sm}^* \times u_{pb}, i_{sc}^* = I_{sm}^* \times u_{pc}. \tag{31}$$

After extracting the reference source currents, the reference DSTATCOM currents will be the difference between the actual load currents and reference source currents.

$$i_{ca}^* = i_{la} - i_{sa}^*; i_{cb}^* = i_{lb} - i_{sb}^*; i_{cc}^* = i_{lc} - i_{sc}^*. \tag{32}$$

Reference DSTATCOM currents at $(k+1)$th state are obtained by applying second order Lagrange extrapolation[14,18] to the DSTATCOM currents in (32).

$$i_c^*(k+1) = 3i_c^*(k) - 3i_c^*(k-1) + i_c^*(k-2) \tag{33}$$

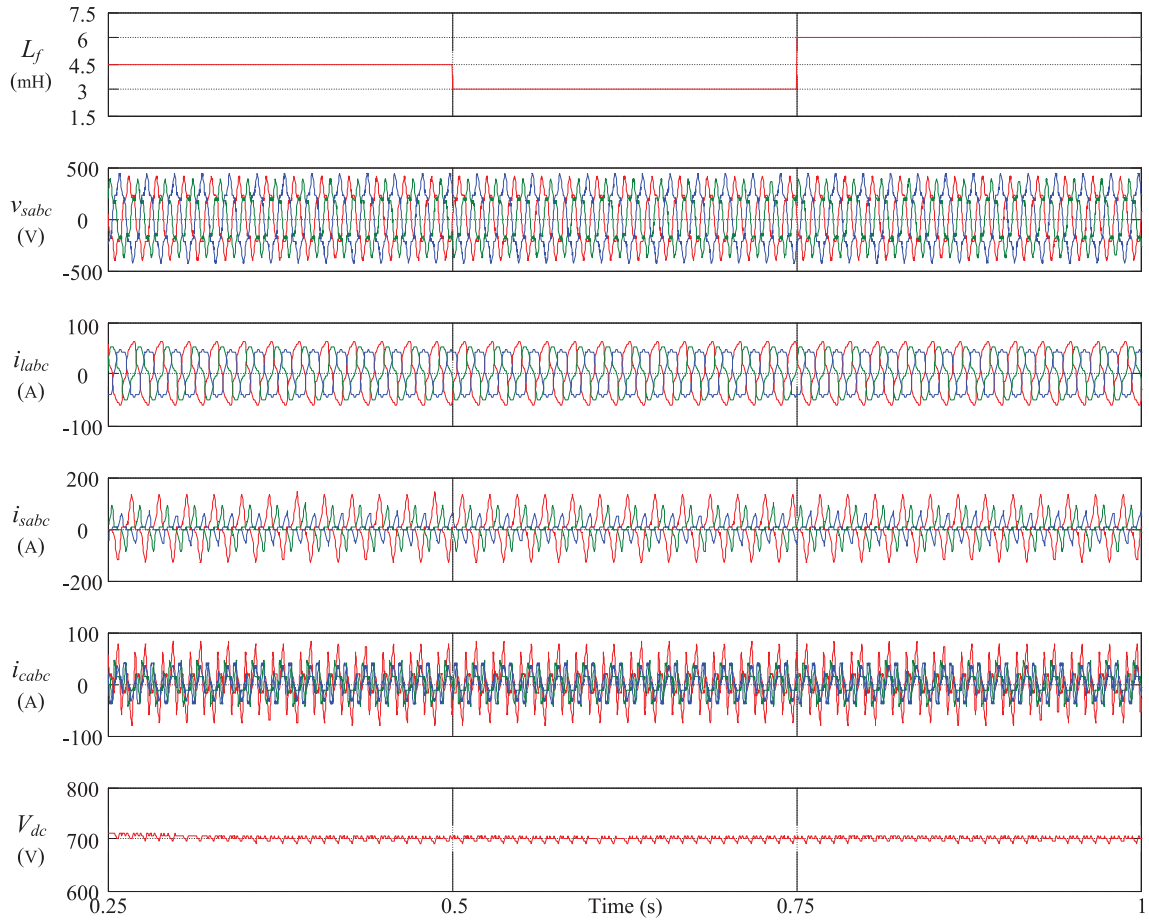

FIGURE 16 Performance during $\sigma_1 = 0.7$ and $\sigma_2 = 0.3$ (Case d)

3 | SIMULATION STUDIES

The assessment of the proposed control algorithm is done using both simulation and experimental studies. Parameters considered for the simulation studies are given in Table 1. Two different cases were considered to test the efficacy of the proposed method. In case-1, a three-phase diode bridge rectifier and a three-phase unbalanced *RL* load is connected. Similarly, in case-2, three single-phase diode bridge rectifiers and a balanced *RL* load is considered to achieve higher total harmonic distortion (THD) load currents.

3.1 | Performance of the proposed method during case-1

In this case, performance of the proposed method (two constraints) is compared with the conventional method (single constraint).[21] Figure 6 shows voltages and currents of the DSTATCOM and distribution system during transition from conventional method to the proposed method. The average switching frequencies of upper switches in each leg are measured for both conventional and proposed methods and the values are mentioned in Table 2. In the same table root mean square (RMS) values and THDs of PCC voltages, load currents and source currents are also mentioned. The RMS values of PCC voltages are 239.3 V, 213.8 V and 261.7 V; similarly, the % distortions are 20.29, 24.84 and 16.62. These values indicate that the PCC voltages are unbalanced as well as distorted. The RMS values of load currents are 43.16 A, 34.66 A and 35.38 A with THDs 16.11%, 22.81% and 17.34% respectively. From these values, it is observed that the load currents are non-linear and also unbalanced. After compensation, with conventional method, the RMS values of source currents are 31.65 A, 31.64 A and 31.64 A respectively with THDs 1.68%, 1.54% and 1.57% which indicate that the source currents become balanced and sinusoidal, which can be also observed from Figure 6. However, from Table 2, it is observed that the switching frequency of the neutral leg is much higher compared to phase leg. After including

TABLE 4 Power quality indices with inductance parameter deviation for different weight factors

Values of σ	L_f (mH)	v_{sa} (V)	v_{sb} (V)	v_{sc} (V)	i_{la} (A)	i_{lb} (A)	i_{lc} (A)	i_{sa} (A)	i_{sb} (A)	i_{sc} (A)	S_n (Hz)
$\sigma_1 = 1$ $\sigma_2 = 0$	3	239.3 (20.29%)	213.8 (24.84%)	261.7 (16.62%)	43.16 (16.11%)	34.66 (22.81%)	35.38 (17.34%)	31.65 (2.00%)	31.72 (1.84%)	31.59 (1.78%)	
	4.5	239.3 (20.29%)	213.8 (24.84%)	261.7 (16.62%)	43.16 (16.11%)	34.66 (22.81%)	35.38 (17.34%)	31.82 (1.60%)	31.86 (1.66%)	31.78 (1.44%)	29 690
	6	239.3 (20.29%)	213.8 (24.84%)	261.7 (16.62%)	43.16 (16.11%)	34.66 (22.81%)	35.38 (17.34%)	31.7 (1.46%)	31.74 (1.54%)	31.69 (1.34%)	
$\sigma_1 = 0.9$ $\sigma_2 = 0.1$	3	239.3 (20.29%)	213.8 (24.84%)	261.7 (16.62%)	43.16 (16.11%)	34.66 (22.81%)	35.38 (17.34%)	31.66 (2.10%)	31.67 (1.85%)	31.61 (1.90%)	
	4.5	239.3 (20.29%)	213.8 (24.84%)	261.7 (16.62%)	43.16 (16.11%)	34.66 (22.81%)	35.38 (17.34%)	31.84 (1.87%)	31.81 (1.81%)	31.76 (1.71%)	17 206
	6	239.3 (20.29%)	213.8 (24.84%)	261.7 (16.62%)	43.16 (16.11%)	34.66 (22.81%)	35.38 (17.34%)	31.74 (2.01%)	31.71 (2.18%)	31.7 (1.85%)	
$\sigma_1 = 0.8$ $\sigma_2 = 0.2$	3	239.2 (20.31%)	213.8 (24.87%)	261.6 (16.63%)	43.16 (16.11%)	34.66 (22.81%)	35.38 (17.34%)	31.64 (2.57%)	31.77 (3.10%)	31.66 (2.35%)	
	4.5	239.2 (20.31%)	213.8 (24.87%)	261.6 (16.63%)	43.16 (16.11%)	34.66 (22.81%)	35.38 (17.34%)	31.81 (2.27%)	31.72 (2.16%)	31.81 (2.02%)	11 039
	6	239.2 (20.31%)	213.8 (24.87%)	261.6 (16.63%)	43.16 (16.11%)	34.66 (22.81%)	35.38 (17.34%)	31.75 (2.64%)	31.56 (2.27%)	31.71 (2.13%)	
$\sigma_1 = 0.7$ $\sigma_2 = 0.3$	3	237.2 (20.71%)	213.1 (24.35%)	261.2 (16.22%)	42.92 (16.28%)	34.65 (22.89%)	35.16 (17.18%)	58.87 (47.99%)	31.89 (66.10%)	20.61 (60.51%)	
	4.5	237.2 (20.71%)	213.1 (24.35%)	261.2 (16.22%)	42.92 (16.28%)	34.65 (22.89%)	35.16 (17.18%)	57.22 (49.14%)	31.46 (67.61%)	20.66 (62.61%)	195
	6	237.2 (20.71%)	213.1 (24.35%)	261.2 (16.22%)	43.16 (16.11%)	34.66 (22.81%)	35.38 (17.34%)	57.75 (48.84%)	31.2 (68.33%)	20.65 (63.25%)	

switching frequency reduction constraint, the switching frequency of the neutral leg is reduced from 29 690 Hz to 11 039 Hz which is almost a 62% reduction. As mentioned, the reduction in neutral leg switching frequency will also reduce the frequencies of phase legs and the reduced values are mentioned in Table 2. At the same time, the RMS values of source currents with the proposed method are 31.74 A, 31.53 A and 31.7 A with THDs 2.68%, 2.08% and 2.25% respectively, indicating that the source currents are balanced and the THD values are also well under the limits of IEEE 519-1992 standard. The reduction in switching frequency causes a slight deviation from actual current tracking which is observed from the zoomed part in Figure 6. From the zoomed figure it is observed that, even though the tracking accuracy is reduced, there is no considerable variation in the neutral current. During the entire operation the DC link voltage is maintained constant (equal to 700 V) and it is shown in Figure 6.

3.1.1 | Comparison with VIKOR method[19]

Performance of the proposed control algorithm is also compared with MPC with VlseKriterijumska Optimizacija I Kompromisno Resenje (VIKOR) method[19] and it is shown in Figure 7. From the figure, it is observed that, the performance of the FL-DSTATCOM with VIKOR method is nearly similar to TOPSIS method. RMS values, THD's and switching frequencies with conventional MPC,[21] VIKOR-based MPC and proposed control algorithm are shown in Table 2. From this table, it is observed that, the reduction in switching frequency with VIKOR method is less compared TOPSIS method. From the above results and analysis it is observed that the performance of the proposed TOPSIS method is better compared to conventional MPC and VIKOR-based MPC.

3.2 | Performance of the proposed method during case-2

In this case, simulation time is considered as 0.4 second. From (0-0.2) second FL-DSTATCOM is not connected to the distribution system. At 0.2 second FL-DSTATCOM is connected to the distribution system and it is operated with the proposed method. Performance of the proposed method, with and without connecting FL-DSTATCOM to the distribution system is shown in Figure 8. From this figure, it is observed that, during (0-0.2) second, load currents and source currents are same and there are no DSTATCOM currents. At 0.2 second FL-DSTATCOM is connected, so that the source currents become balanced and sinusoidal.

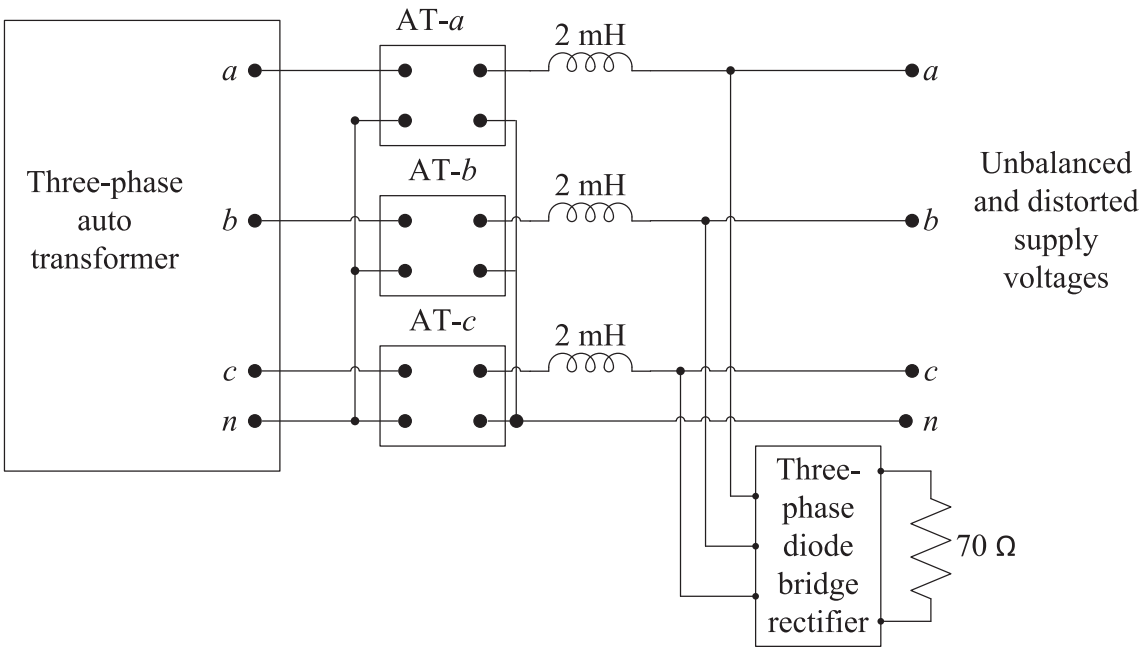

FIGURE 17 Realization of three-phase unbalanced and distorted supply

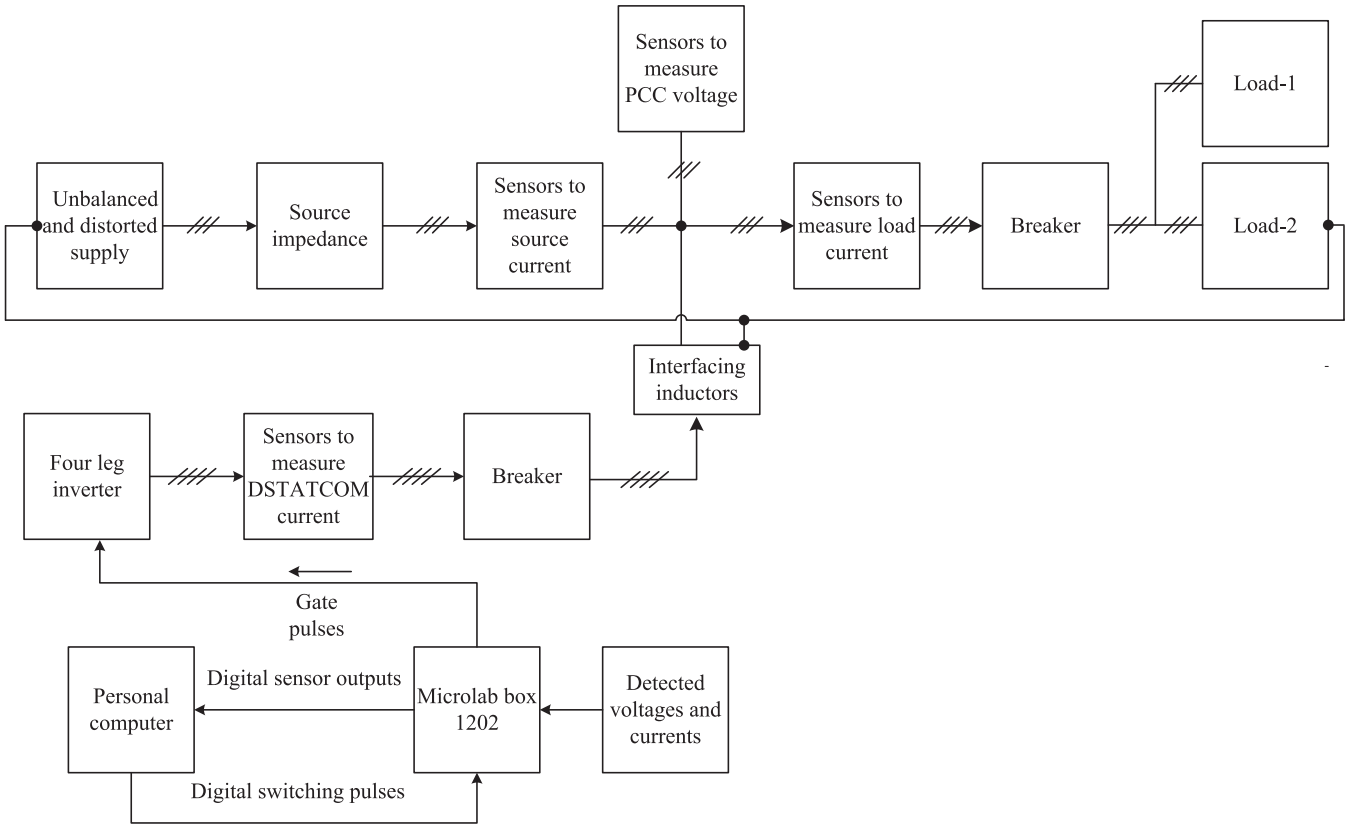

FIGURE 18 Connection block diagram to implement the experimental prototype

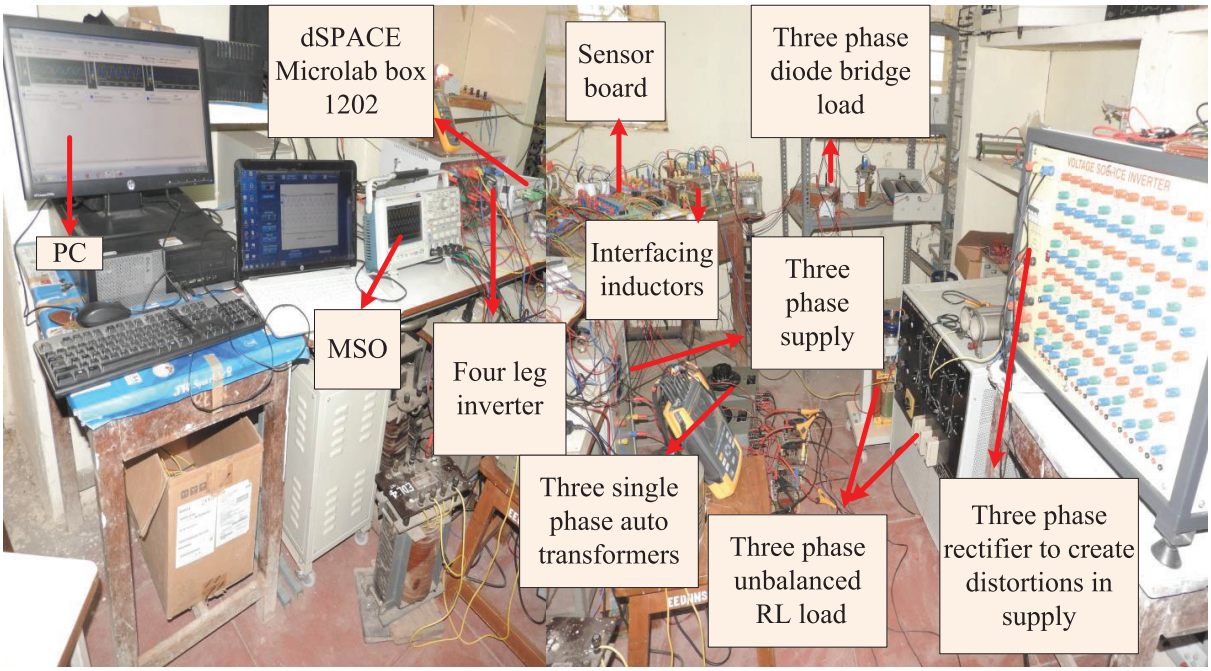

FIGURE 19 Photograph of experimental setup

3.2.1 | Comparison with conventional method

The performance of the proposed method is also determined for load currents with higher unbalance and higher THDs. Loads considered in case-2 are mentioned in Table 1. Figure 9 shows the simulation results with conventional[21] and the proposed methods during case-2. From this figure, it is observed that, the performance of the proposed method is satisfactory during high THD and unbalance in load currents. RMS values as well as THDs of PCC voltages, load currents, source currents and switching frequencies of each leg are mentioned in Table 3 for both conventional and proposed methods. It is observed that the source currents are balanced and sinusoidal even though the supply voltage and load currents are unbalanced and distorted. Figures 10 and 11 show the average switching frequency of each leg with

TABLE 5 Experimental setup parameters

Parameters	Value
Unbalanced Supply voltage	$V_{sa} = 28 \times 1.25$ V, $V_{sb} = 28$ V, $V_{sc} = 28 \times 0.75$ V.
Interfacing inductance	$L_f = 9$ mH
DC link capacitance	$C_{dc} = 4700\ \mu$F
DC Link voltage	$V_{dc} = 90$ V
Load-1	Three-phase diode bridge rectifier load with 30 Ω, 150 mH
Load-2	Unbalanced linear load
	Phase-*a*: 18 Ω, 75 mH, Phase-*b*: 18 Ω, 50 mH, Phase-*c*: 18 Ω, 100 mH

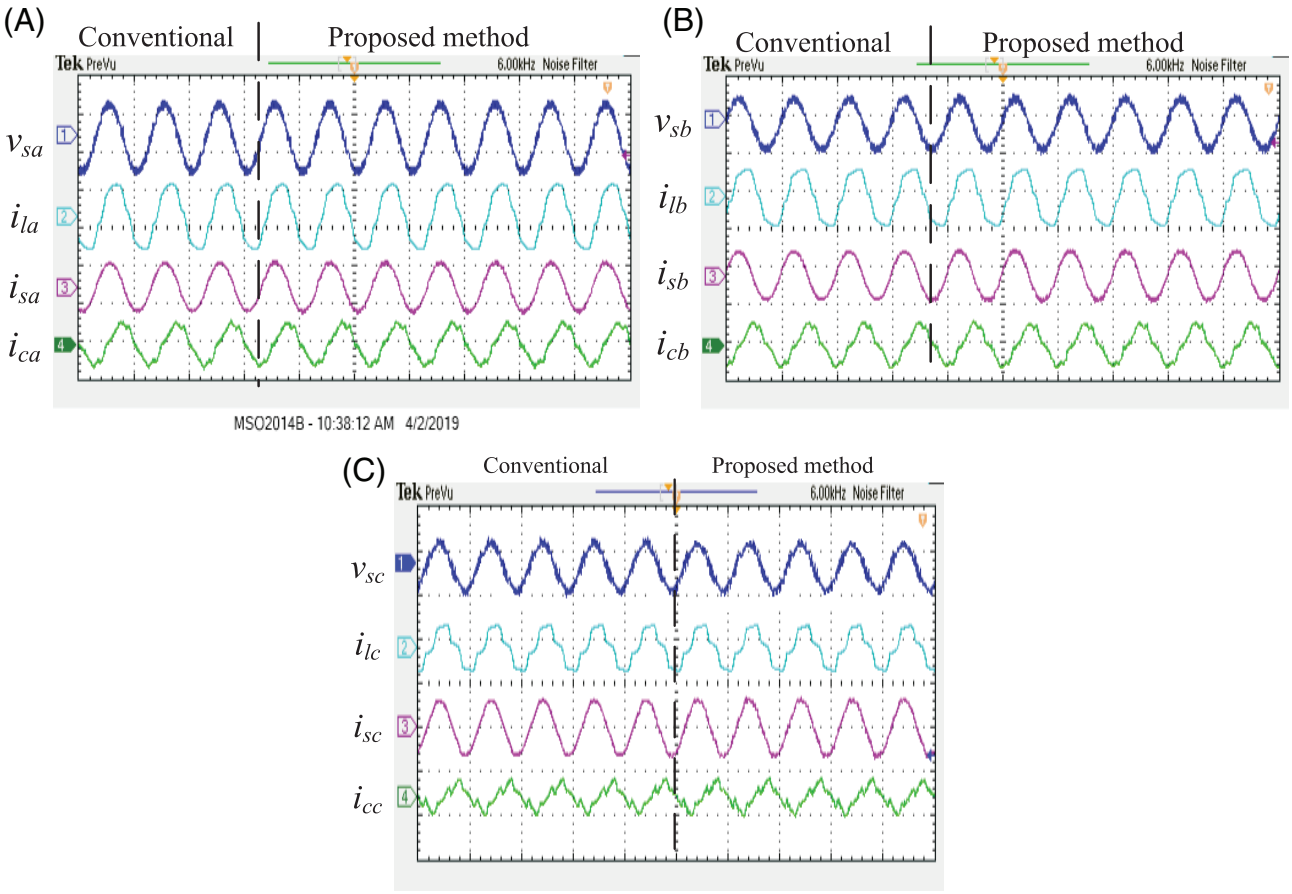

FIGURE 20 Voltages and currents of (A) Phase-*a* (B) Phase-*b* and (C) Phase-*c*

conventional and proposed methods. The average switching frequencies are calculated from these figures and they are mentioned in Table 3. From this table, it is observed that the proposed method reduced the switching frequency of neutral leg from 27 752 Hz to 10 108 Hz (63%). Neutral currents of load, DSTATCOM and source are shown in Figure 12 and it is observed that the number of switching pulses is reduced after adding switching frequency reduction constraint. Similarly, source neutral current is almost zero during both single and multiple constraints.

The simulation results during case-1 and case-2 indicate that the proposed control algorithm renders source current balanced and sinusoidal irrespective of the distortion in either source or load. It also reduces the switching frequency of the neutral leg which reduces further the switching frequencies of phase legs without much variation in the source neutral current.

3.3 | Parameter sensitivity analysis

Weighting factors considered in the proposed control algorithm are $\sigma_1 = 0.8$, $\sigma_2 = 0.2$ and inductance value (L_f) considered as 0.45 mH. At the same time, the other values of weighting factors considered for comparison are ($\sigma_1 = 1$, $\sigma_2 = 0$), ($\sigma_1 = 0.9$, $\sigma_2 = 0.1$), and ($\sigma_1 = 0.7$, $\sigma_2 = 0.3$). Similarly, the other inductance values considered are 0.3 mH, and 0.6 mH. Figures 13, 14, 15, and 16 are showing the simulation results with different weighting factor values and different L_f values. Table 4 is showing the RMS values and THDs of voltages and currents along with the switching frequencies of inverter switches.

Case a ($\sigma_1 = 1$, $\sigma_2 = 0$): The weighting factor values considered in this case are reflecting the conventional MPC, where complete importance is given to current control. From Table 4 it is observed that, if the inductance value varies from the real time value, there is slight change in the THD of source current. In this case, the calculated value of neutral leg switching frequency is 29 690 Hz.

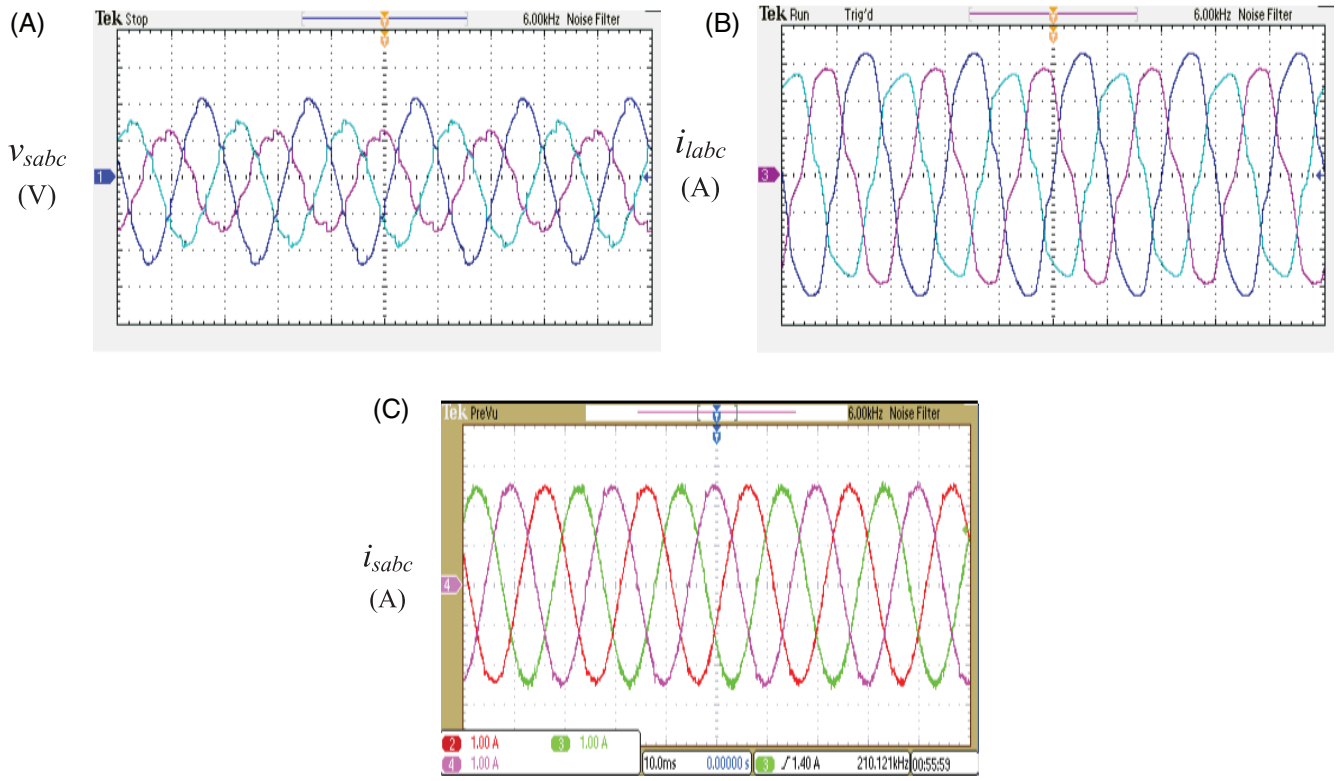

FIGURE 21 (A) Unbalanced and distorted PCC voltages, (B) unbalanced and distorted load currents and (C) balanced and sinusoidal source currents

Case b ($\sigma_1 = 0.9, \sigma_2 = 0.1$): In this case, weighting factor for current control (σ_1) and neutral leg switching frequency reduction (σ_2) are considered as 0.9 and 0.1. From Table 4 it is observed that, due to $\sigma_2 = 0.1$, the switching frequency of the neutral leg is reduced to 17 206 Hz (42% reduced compared to previous case).

Case c ($\sigma_1 = 0.8, \sigma_2 = 0.2$): Weighting factor for current control (σ_1) and neutral leg switching frequency reduction (σ_2) are considered as 0.8 and 0.2 and they are same as proposed control algorithm. Due to $\sigma_2 = 0.2$, the switching frequency of the neutral leg is further reduced and the value is 11 309 Hz (34% reduction compared to case ii.) The reduction in frequency causes a slight increase in the THD of source current. However, the increased THD are well under the limits of IEEE standards.

Case d ($\sigma_1 = 0.7, \sigma_2 = 0.3$): Weighting factor for current control (σ_1) and neutral leg switching frequency reduction (σ_2) are considered as 0.7 and 0.3. The increased importance to switching frequency reduction constraint ($\sigma_2 = 0.3$) causes the sudden fall-down of the neutral leg switching frequency and its value is equal to 195 Hz (98% reduction compared to case iii). Because of this lower neutral leg switching frequency, switches of the FL-DSTATCOM loose its control which leads to poor performance of the proposed control algorithm. The THD values of source currents are 49.14%, 67.61%, and 62.61% indicates that the performance of the proposed control algorithm is very poor and also not efficient. Voltages and various currents during this case are shown in Figure 16. From the figure, it is observed that, the source currents are not balanced and sinusoidal with $\sigma_1 = 0.7$, $\sigma_2 = 0.3$.

From the above analysis, it is observed that

1. The variation in L_f value from the real time value causes, a slight change in THD of source current, which does not effect the performance of the proposed control algorithm.

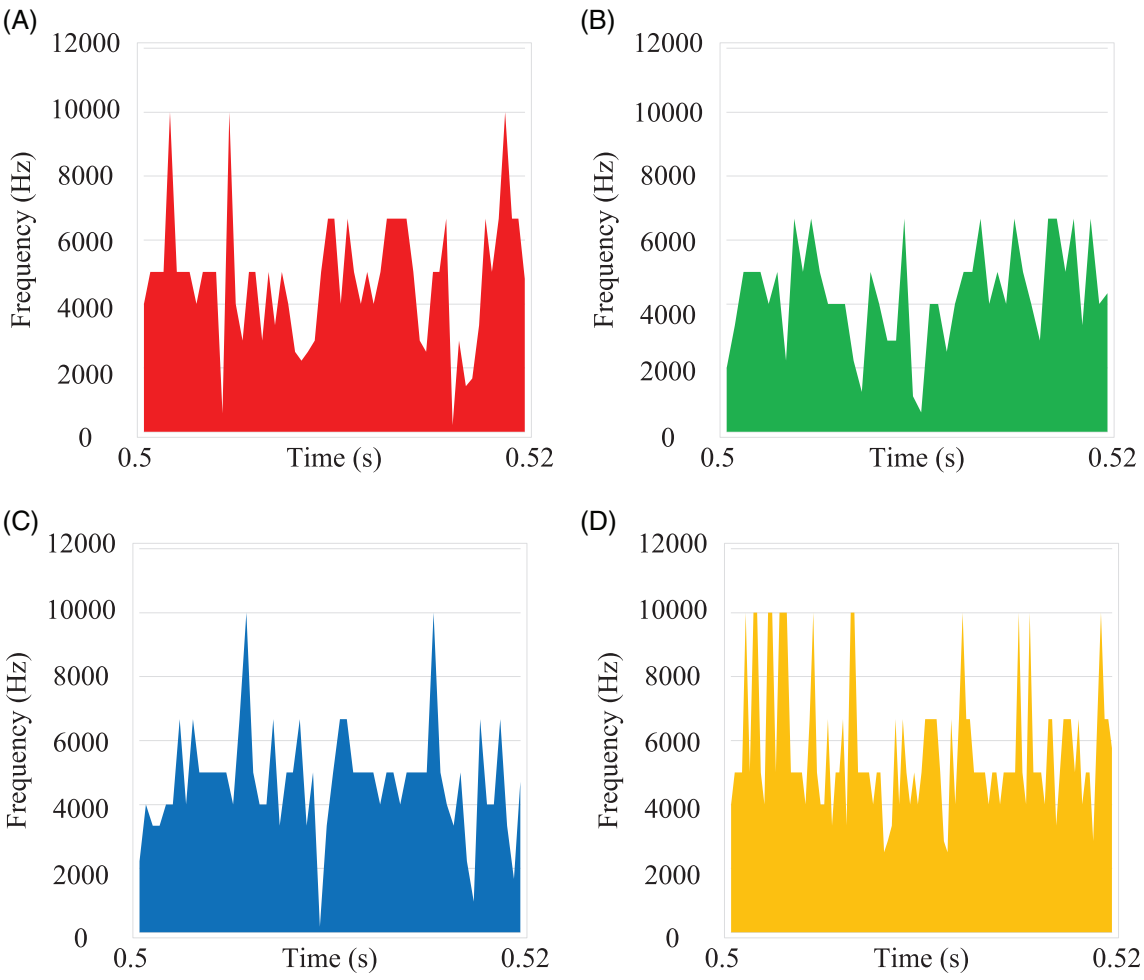

FIGURE 22 Switching frequency with conventional method for (A) Phase-*a* (B) Phase-*b* (C) Phase-*c* and (D) Neutral leg

2. However, during $\sigma_1 = 0.7$, $\sigma_2 = 0.3$, neutral leg switching frequency is almost zero and performance of the proposed control algorithm is very poor.

4 | EXPERIMENTAL STUDIES

The effectiveness of the proposed control algorithm is also evaluated through experimental studies. Three-phase unbalanced and distorted supply is required to establish the experimental prototype. The unbalanced and distorted supply is created using a combination of three-phase auto transformer, three single-phase auto transformers, a three-phase diode bridge rectifier and three inductors. The connection diagram of unbalanced and distorted supply is shown in Figure 17. Initially three single-phase auto transformers are supplied by a three-phase auto transformer. Then the three single-phase transformers are maintained at unequal voltages to get unbalanced supply. The unbalanced three-phase supply is connected to a three-phase diode bridge rectifier feeding an *R* load through inductors. The terminal points of the inductors are as shown in Figure 17, which provides the required unbalanced and distorted supply for the experimental setup. The connection diagram of the experimental setup is shown in Figure 18. Photograph of the complete experimental setup is shown in Figure 19. The other required parameters for the experimental test are mentioned in Table 5. Initially Liaisons Electroniques et Mecaniques made current and voltage sensors are used to sense the load currents, DSTATCOM currents and PCC voltages. The sensed signals are send to personnel computer (PC) using dSPACE MicroLab Box 1202 which acts as an interfacing device. After sending the detected signals to the PC, the proposed con-

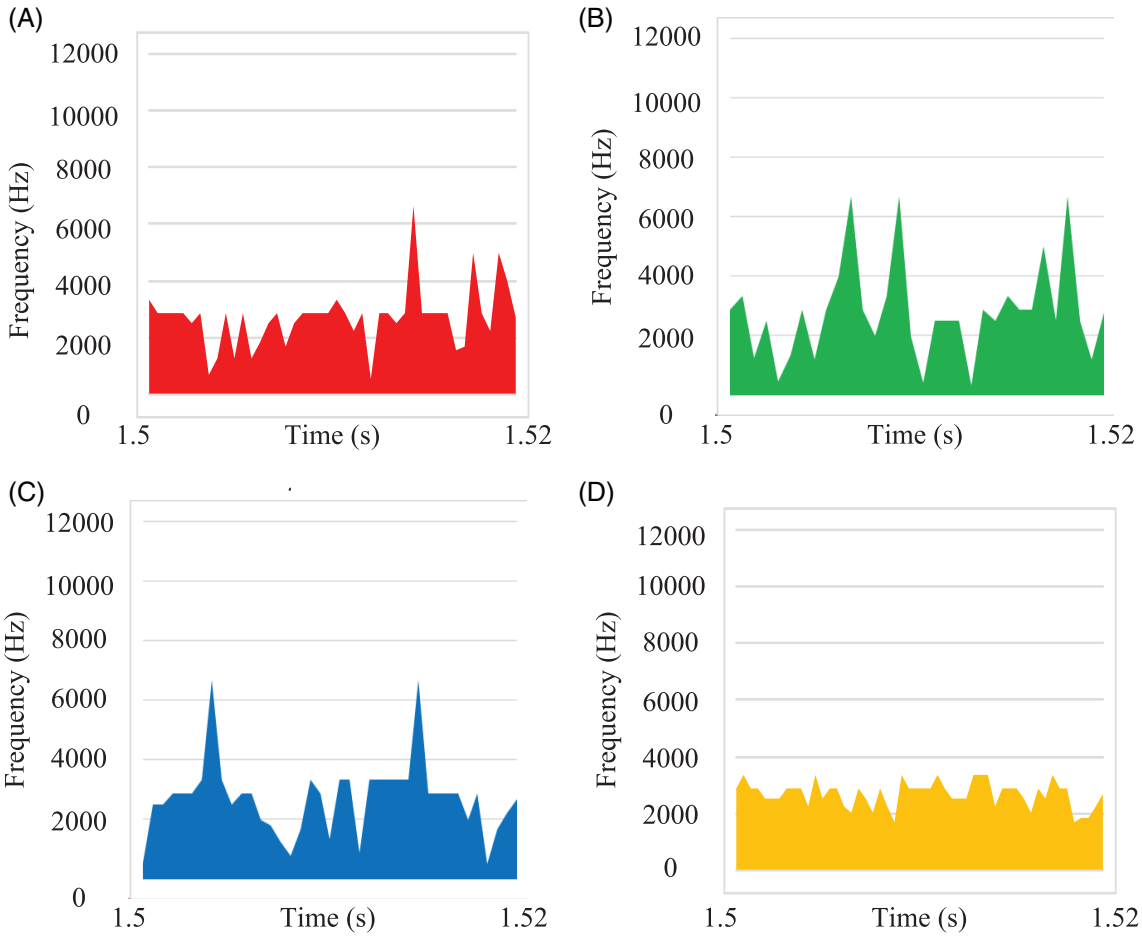

FIGURE 23 Switching frequency with proposed method for (A) Phase-*a* (B) Phase-*b* (C) Phase-*c* and (D) Neutral leg

trol algorithm is implemented and the generated gate pulses are given to FL-DSTATCOM using dSPACEMicroLab Box 1202.

Experimental results of voltages, load currents and source currents are shown in Figure 20. In this figure voltage scaling is 50 V/div and current scaling is 4 A/div. Figure 20A-C shows parameters of phase-*a*, phase-*b* and phase-*c* respectively. From this figure, it is observed that, even though the cost function varies from single constraint to multiple

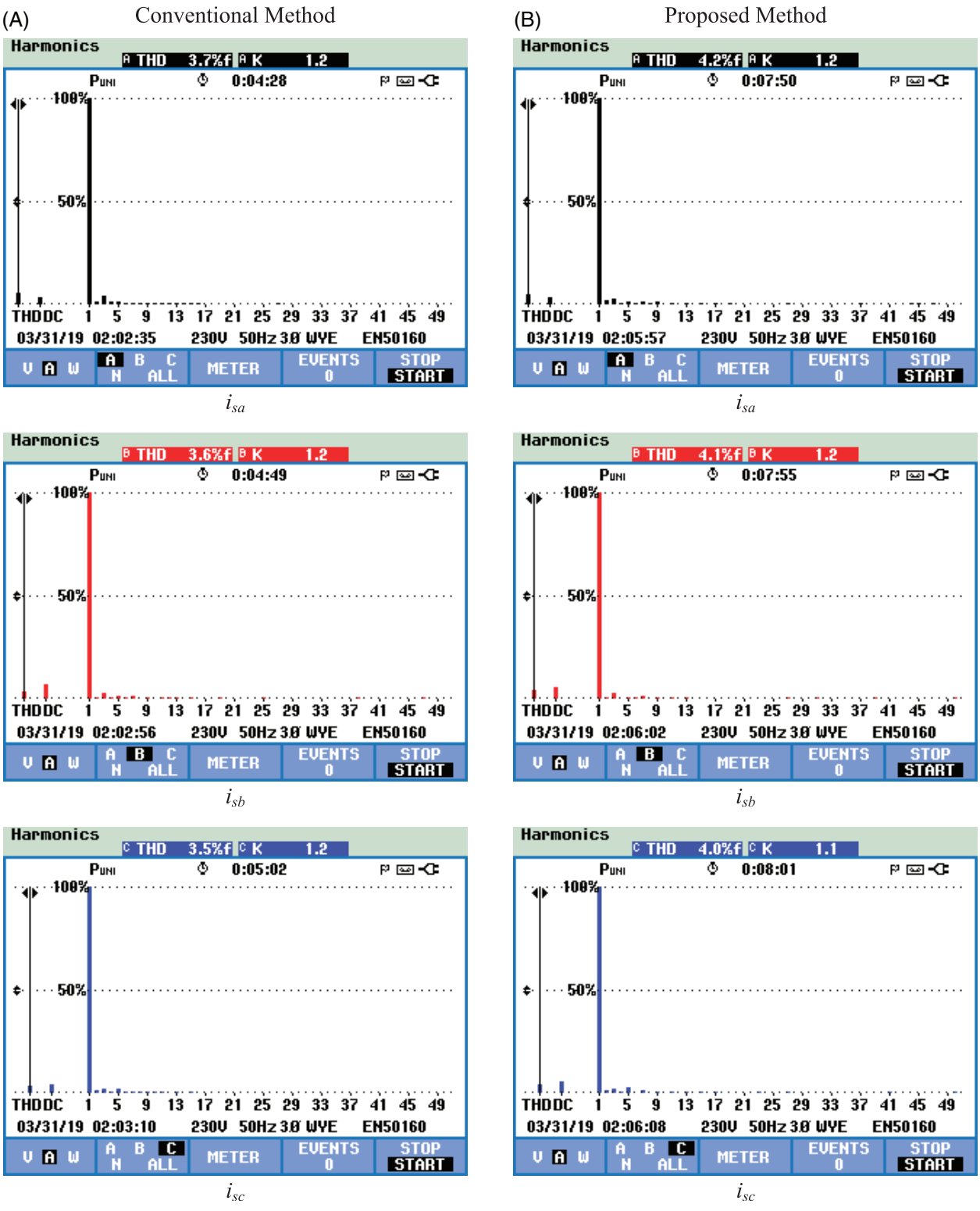

FIGURE 24 THDs of source currents with (A) Conventional method and (B) Proposed method

constraints there is not much variation in the performance of the proposed control algorithm. Figure 21 shows PCC voltages, load currents and source currents of three phases. In Figure 21A, voltage scaling is 20 V/div, In Figure 21B,C current scaling is 1 A/div. It is observed from Figure 21A that the supply voltage is unbalanced and distorted, Figure 21B shows that load currents are non-linear and unbalanced. After compensation the source currents become balanced and sinusoidal and as observed from Figure 21C. Figure 22 shows the switching frequencies of neutral leg along with the individual phases. The frequencies of phase-*a*, phase-*b* and phase-*c* with conventional method are 4785 Hz, 4366 Hz and 4711 Hz and they are shown as Figure 22A-C. The neutral leg switching frequency is 5770 Hz which is higher compared to phase legs and is shown in Figure 22D. As mentioned earlier, the higher neutral leg frequency is reduced by adding an additional constraint to the cost function. The neutral leg switching frequency with the proposed method is 2661 Hz which is lower compared to the conventional method. This reduction in neutral leg switching frequency also reduces the switching frequency of phase legs with the reduced frequencies being 2703 Hz, 2794 Hz and 2671 Hz for phase-*a*, phase-*b* and phase-*c* respectively. The switching frequencies after adding additional constraints are shown in Figure 23. The THD of source currents with conventional and proposed methods are shown in Figure 24. From this figure it is observed that the THD of source currents are 3.7%, 3.6% and 3.5% with only current control. After adding switching frequency constraint the THDs are 4.2%, 4.1% and 4.0% respectively which are within the limits set by IEEE standards (less than 5%). The computational time with conventional method (MPC with only current control),[21] proposed TOPSIS method and VIKOR method[19] are obtained as 36 microseconds, 41 microseconds and 48 microseconds. The computational time for the proposed method is slightly high (5 microseconds) with respect to conventional MPC, less (7 microseconds) with respect to VIKOR-based MPC.

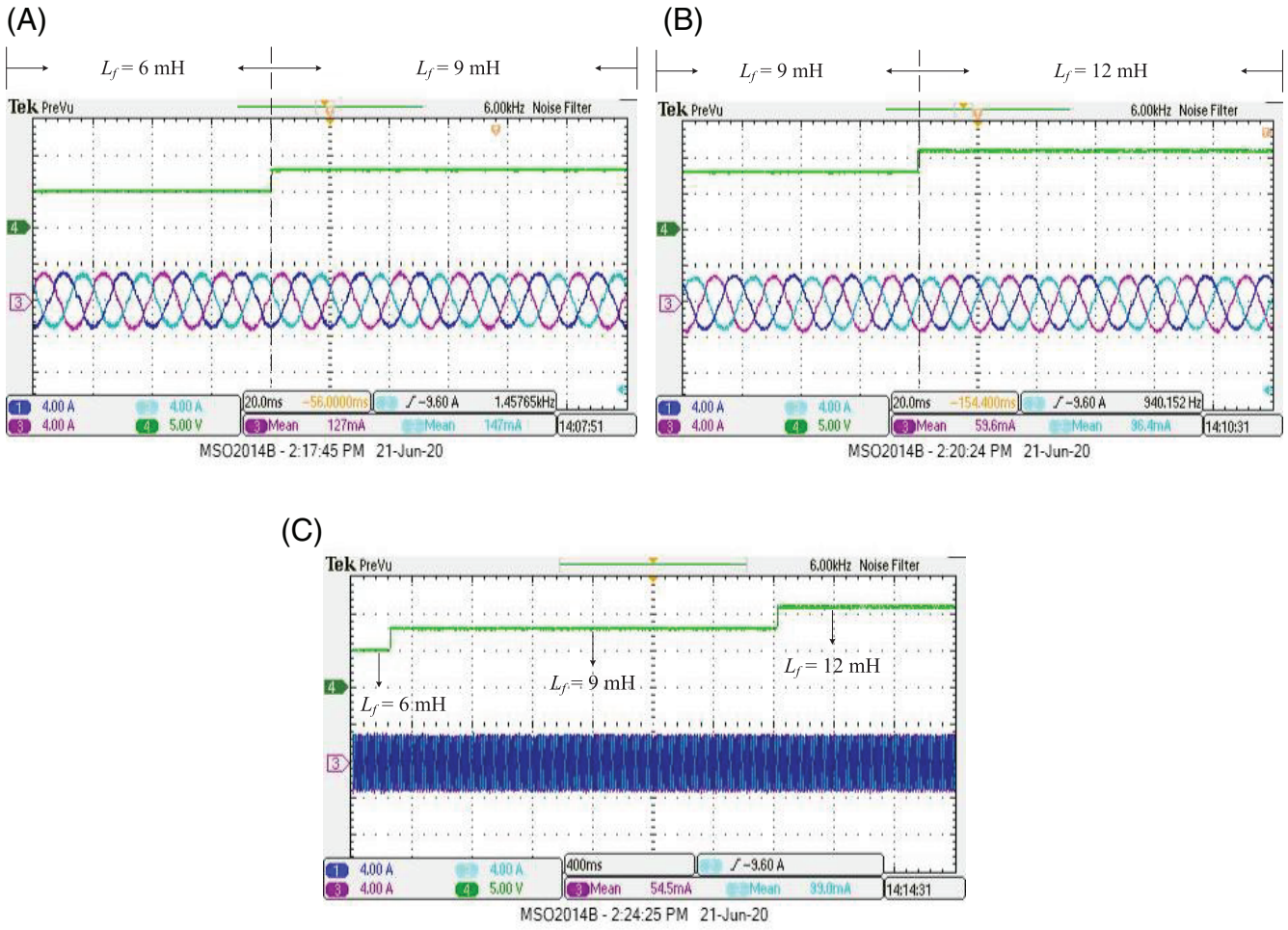

FIGURE 25 Source current with variation in L_f (A) L_f varies from 6 mH to 9 mH (B) L_f varies from 9 mH to 12 mH Phase-*b*, and (C) L_f varies from (6-9-12) mH

4.1 | Parameter sensitivity analysis

The cost function of the proposed work consists of minimization of current error (as mentioned in (5)) and switching state difference (as mentioned in (6)). From (4) and (5), it is observed that that the predicted values of compensator currents are dependent on the ratio of sampling time (T_s), interfacing inductance (L_f). During experimental studies, T_s is considered as 50 microseconds, L_f is considered as 9 mH. If there is a 3 mH variation in the L_f, the obtained values of L_f are 6 mH and 12 mH. The calculated values of $\frac{T_s}{L_f}$ for various L_f are,

$$\left(\frac{T_s}{L_f}\right)_{L_f=6\,\mathrm{mH}} = 0.00833; \left(\frac{T_s}{L_f}\right)_{L_f=9\,\mathrm{mH}} = 0.00555; \left(\frac{T_s}{L_f}\right)_{L_f=12\,\mathrm{mH}} = 0.00416. \tag{34}$$

From (34), it is observed that, even though the variation in the L_f is 3 mH, there is not much variation in the values of $\frac{T_s}{L_f}$. Similarly, From (6), it is observed that C_2 is dependent only on present and previous switching state and it is also a parameter independent constraint. Figure 25 shows the source currents during varies values of L_f. From the figure, it is observed that, even though there is a variation in L_f there is no observable change in the source currents. Therefore, parameter variation will not effect the performance of the proposed control algorithm.

5 | CONCLUSION

This paper dealt primarily with compensation of current-related power quality issues using FL-DSTATCOM and neutral leg switching frequency reduction of FL-DSTATCOM. Initially, DSTATCOM currents were predicted using model of the FL-DSTATCOM. Then, the difference between reference and actual DSTATCOM currents is considered as a cost function to compensate for current-related power quality issues. The higher neutral leg switching frequency, which is one of the limitations of FL-DSTATCOM is reduced by adding an additional constraint to the cost function. The complexity in the weighting factor tuning for optimal switching state selection during multi-constraint case is simplified using TOPSIS method by reducing its range from $(0 - \infty)$ to (0-1). The reduction in neutral leg switching frequency is 62% during simulation and 53% during experimental studies. Finally, the complexity in the extraction of reference currents during unbalance and distorted supply conditions is reduced using state observers and theory of symmetrical components.

PEER REVIEW

The peer review history for this article is available at https://publons.com/publon/10.1002/2050-7038.12688.

DATA AVAILABILITY STATEMENT

Data sharing is not applicable to this article as no new data were created or analyzed in this study.

ORCID

Siva Kumar Ganjikunta https://orcid.org/0000-0001-5512-5669

REFERENCES

1. Singh B, Chandra A, Al-Haddad K. *Power Quality: Problems and Mitigation Techniques*. Chichester, England: John Wiley & Sons; 2014.
2. Sreenivasarao D, Agarwal P, Das B. Neutral current compensation in three-phase, four-wire systems: a review. *Electr Power Syst Res*. 2012;86:170-180.
3. Patel SK, Arya SR, Maurya R, Jain C, Singh B. Control of distributed static compensator using extended structure-enhanced phase-locked loop-based algorithm under nonideal AC mains. *Int Trans Electr Energy Syst*. 2017;27(9):e2354.
4. Badoni M, Singh A, Singh B. An implementation of variable step-size least-mean-square based control algorithm for DSTATCOM. *Int Trans Electr Energy Syst*. 2016;26(7):1540-1554.
5. Mohamed SA. Enhancement of power quality for load compensation using three different FACTS devices based on optimized technique. *Int Trans Electr Energy Syst*. 2019;13(7):e12196.
6. Barghi Latran M, Teke A, Yoldaş Y. Mitigation of power quality problems using distribution static synchronous compensator: a comprehensive review. *IET Power Electron*. 2015;8(7):1312-1328.
7. Mahela OP, Shaik AG. A review of distribution static compensator. *Renew Sustain Energy Rev*. 2015;50:531-546.

8. Manoj Kumar MV, Mishra MK. Three-leg inverter-based distribution static compensator topology for compensating unbalanced and non-linear loads. *IET Power Electron*. 2015;8(11):2076-2084.
9. Manoj Kumar MV, Mishra MK. Dual distribution static compensator for three-phase four-wire distribution system. *IET Gener Transm Distrib*. 2016;10(2):399-411.
10. Khadkikar V, Chandra A, Singh B. Digital signal processor implementation and performance evaluation of split capacitor, four-leg and three H-bridge-based three-phase four-wire shunt active filters. *IET Power Electron*. 2011;4(4):463-470.
11. Singh B, Arya SR, Jain C, Goel S. Implementation of four-leg distribution static compensator. *IET Gener Transm Distrib*. 2014;8(6):1127-1139.
12. Dheepanchakkravarthy A, Selvan MP, Moorthi S. Alleviation of power quality issues caused by electric arc furnace load in power distribution system using 3-phase four-leg DSTATCOM. *J Inst Eng B*. 2019;100(1):9-22.
13. Dheepanchakkravarthy A, Akhil S, Venkatraman K, Selvan MP, Moorthi S. Performance analysis of FPGA controlled four-leg DSTATCOM for multifarious load compensation in electric distribution system. *Eng Sci Technol*. 2018;21(4):692-703.
14. Vazquez S, Rodriguez J, Rivera M, Franquelo LG, Norambuena M. Model predictive control for power converters and drives: advances and trends. *IEEE Trans Indus Electron*. 2017;64(2):935-947.
15. Kouro S, Perez MA, Rodriguez J, Llor AM, Young HA. Model predictive control: MPC's role in the evolution of power electronics. *IEEE Indus Electron Mag*. 2015;9(4):8-21.
16. Kanagavel R, Vairavasundaram I, Padmanaban S. Design and prototyping of single-phase shunt active power filter for harmonics elimination using model predictive current control. *Int Trans Electr Energy Syst*. 2019;30(2):e12231.
17. Panigrahi R, Subudhi B, Panda PC. Model predictive-based shunt active power filter with a new reference current estimation strategy. *IET Power Electron*. 2015;8(2):221-233.
18. Venkatraman K, Selvan MP, Moorthi S. Predictive current control of distribution static compensator for load compensation in distribution system. *IET Gener Transm Distrib*. 2016;10(10):2410-2423.
19. Pranay Kumar A, Siva Kumar G, Sreenivasarao D, Myneni H. Model predictive current control of DSTATCOM with simplified weighting factor selection using VIKOR method for power quality improvement. *IET Gener Trans Distrib*. 2019;13(16):3649-3660.
20. Yaramasu V, Rivera M, Wu B, Rodriguez J, et al. Model predictive current control of two-level four-leg inverters—part I: concept, algorithm, and simulation analysis. *IEEE Trans Power Electron*. 2012;28(7):3459-3468.
21. Dheepanchakkravarthy A, Jawahar MR, Venkatraman K, Selvan MP, Moorthi S. Performance evaluation of FPGA-based predictive current controller for FL-DSTATCOM in electric distribution system. *IET Gener Transm Distrib*. 2019;13(19):4400-4409.
22. Lohia P, Mishra MK, Karthikeyan K, Vasudevan K. A minimally switched control algorithm for three-phase four-leg VSI topology to compensate unbalanced and nonlinear load. *IEEE Trans Power Electron*. 2008;23(4):1935-1944.
23. Cortés P, Kouro S, La Rocca B, Vargas R, Rodríguez J, León JI, Vazquez S, Franquelo LG. Guidelines for weighting factors design in model predictive control of power converters and drives. Paper presented at: 2009 IEEE International Conference on Industrial Technology; 2009:1-7.
24. Tzeng GH, Huang JJ. *Multiple Attribute Decision Making: Methods and Applications*. Boca Raton, FL: Chapman and Hall/CRC; 2011.
25. Kanjiya P, Khadkikar V, Zeineldin HH. Optimal control of shunt active power filter to meet IEEE Std. 519 current harmonic constraints under nonideal supply condition. *IEEE Trans Indus Electron*. 2015;62(2):724-734.
26. Patel SK, Arya SR, Maurya R, Singh B. Interior point algorithm for optimal control of distribution static compensator under distorted supply voltage conditions. *IET Gener Trans Distrib*. 2016;10(8):1778-1791.
27. Uyyuru KR, Mishra MK, Ghosh A. An optimization-based algorithm for shunt active filter under distorted supply voltages. *IEEE Trans Power Electron*. 2009;24(5):1223-1232.
28. Rao UK, Mishra MK, Ghosh A. Control strategies for load compensation using instantaneous symmetrical component theory under different supply voltages. *IEEE Trans Power Deliv*. 2008;23(4):2310-2317.
29. Singh B, Solanki J. A comparison of control algorithms for DSTATCOM. *IEEE Trans Indus Electron*. 2009;56(7):2738-2745.
30. Asiminoael L, Blaabjerg F, Hansen S. Detection is key-harmonic detection methods for active power filter applications. *IEEE Indus Appl Mag*. 2007;13(4):22-33.
31. Singh B, Solanki J. A comparative study of control algorithms for DSTATCOM for load compensation. Paper presented at: 2006 IEEE International Conference on Industrial Technology; 2006:1492-1497.
32. Patil KR, Patel HH. Performance of shunt active power filter with DSOGI-FLL under distorted grid voltage. Paper presented at: 2017 Second International Conference on Electrical, Computer and Communication Technologies (ICECCT); 2017:1-6.
33. Sahu G, Mahapatra K. Real time implementation of digital filter on control strategy of DSTATCOM for load compensation under distorted utility condition. Paper presented at: 2013 IEEE Asia Pacific Conference on Postgraduate Research in Microelectronics and Electronics (PrimeAsia); 2013:164-169.
34. Chilipi R, Al Sayari N, Al Hosani K, Fasil M, Beig AR. Third order sinusoidal integrator (TOSSI)-based control algorithm for shunt active power filter under distorted and unbalanced voltage conditions. *Int J Electr Power Energy Syst*. 2018;96:152-162.
35. Badoni M, Singh A, Singh B, Saxena H. Real-time implementation of active shunt compensator with adaptive SRLMMN control technique for power quality improvement in the distribution system. *IET Gener Transm Distrib*. 2020;14(8):1598-1606.
36. Singh B, Arya SR. Composite observer-based control algorithm for distribution static compensator in four-wire supply system. *IET Power Electron*. 2013;6(2):251-260.

37. Chittora P, Singh A, Singh M. Chebyshev functional expansion based artificial neural network controller for shunt compensation. *IEEE Trans Indus Inform*. 2018;14(9):3792-3800.
38. Kannan VK, Rengarajan N. Investigating the performance of photovoltaic based DSTATCOM using I cos Φ algorithm. *Int J Electr Power Energy Syst*. 2014;54:376-386.
39. Gawande SP, Ramteke MR, Pande N. Improved equal current approach for reference current generation in shunt applications under unbalanced and distorted source and load conditions. *IET Gener Transm Distrib*. 2016;10(4):995-1005.
40. Selvajyothi K, Janakiraman PA. Extraction of harmonics using composite observers. *IEEE Trans Power Deliv*. 2008;23(1):31-40.
41. Dirik H, Özdemir M. New extraction method for active, reactive and individual harmonic components from distorted current signal. *IET Gener Transm Distrib*. 2014;8(11):1767-1777.
42. Cominos P, Munro N. PID controllers: recent tuning methods and design to specification. *IEE Proc Control Theory Appl*. 2002;149(1): 46-53.

How to cite this article: Alladi PK, Ganjikunta SK, Dharmavarapu S. Model predictive control with technique for order of preference by similarity to ideal solution method for four leg distribution static compensator to improve power quality and reduce switching frequency. *Int Trans Electr Energ Syst*. 2021;31:e12688. https://doi.org/10.1002/2050-7038.12688